

SE(3)-Equivariant Reconstruction from Light Field

Yinshuang Xu
 University of Pennsylvania
 Philadelphia, United States
 xuyin@seas.upenn.edu

Jiahui Lei
 University of Pennsylvania
 Philadelphia, United States
 leijh@seas.upenn.edu

Kostas Daniilidis
 University of Pennsylvania
 Philadelphia, United States
 kostas@cis.upenn.edu

Abstract

Recent progress in geometric computer vision has shown significant advances in reconstruction and novel view rendering from multiple views by capturing the scene as a neural radiance field. Such approaches have changed the paradigm of reconstruction but need a plethora of views and do not make use of object shape priors. On the other hand, deep learning has shown how to use priors in order to infer shape from single images. Such approaches, though, require that the object is reconstructed in a canonical pose or assume that object pose is known during training. In this paper, we address the problem of how to compute equivariant priors for reconstruction from a few images, given the relative poses of the cameras. Our proposed reconstruction is SE(3)-gauge equivariant, meaning that it is equivariant to the choice of world frame. To achieve this, we make two novel contributions to light field processing: we define light field convolution and we show how it can be approximated by intra-view SE(2) convolutions because the original light field convolution is computationally and memory-wise intractable; we design a map from the light field to \mathbb{R}^3 that is equivariant to the transformation of the world frame and to the rotation of the views. We demonstrate equivariance by obtaining robust results in roto-translated datasets without performing transformation augmentation.

1. Introduction

Classical geometric vision has thoroughly addressed dense reconstruction [27, 28, 30] from multiple views in terms of photo-consistency, geometric constraints, and optimization in the dense recovery of surfaces. The idea of representing a scene purely as a dense point cloud or a surface associated with texture meshes was not allowing for visually compelling rendering. The confluence of vision and graphics brought into use [41] the notion of a light field, earlier introduced as a plenoptic function ([6], among others). Neural Radiance Fields [46] introduced a novel paradigm that would store a single scene in a network that would al-

low during inference the compelling rendering of any novel view. All the above approaches, neural or not, work on a single scene and produce the same reconstruction independent of the chosen world frame.

On the other hand, recent years have seen significant advances in learning-based techniques [63, 73–75] harnessing the power of deep learning for extraction of 3D shape priors from training on images and associated ground-truth shapes, a paradigm known as semantic reconstruction and been extensively used before for parametric models of faces and humans.

There is an obvious need to combine the multiple-view single scene world with the world that generalizes on objects and scenes because we want to exploit the statistics of object shapes to avoid the plethora of views needed in NeRF-like approaches and the associated optimization using inference. Reconstruction via shape priors has been used with multiple views [14, 74, 77], while rendering approaches have also been extended beyond a single scene by learning neural field priors [54, 64].

However, methods above that use priors for reconstruction and/or rendering do not generalize to arbitrary frames of reference. If the frame of reference is transformed with a rigid transformation or the camera frame is rotated, the reconstruction or rendering is not equivariant. While one could tackle this problem by view pooling [49, 75, 79, 80], such a pooling still leaves the network to be sensitive to each camera orientation and cause information loss.

In this paper, we address the problem of equivariance in 3D reconstruction from multiple views. This SE(3)-equivariance is with respect to the choice of 3D reference coordinate system. Our model is also equivariant to an independent rotation of every camera. Unlike the case of dense reconstruction from point clouds, we are careful not to claim equivariance with respect to object pose or camera position because such changes do not constitute transitive group actions due to the appearance or occlusion of new views of the object. However, we experimentally show that the proposed SE(3)-equivariance approach is robust to bounded 3D content changes due to object pose variation.

We tackle $SE(3)$ equivariant reconstruction in two steps. In the first step, we construct a light feature field that is $SE(3)$ equivariant. In practice, multiple-view sampling cannot yield a continuous light field. However, the strict equivariance is not broken when the sampling content is not changed, which is also the case in the point cloud sampling of a 3D shape. We show, how a convolution on a sparse light field is equivalent to an independent spherical convolution for each camera when the receptive fields of the convolution in the ray space are disjoint across cameras. This convolution can then be approximated via an $SE(2)$ -convolution when the field of view is small, and the image can be regarded as the tangent plane to the image sphere.

The result of the first step is a field with an equivariant feature associated with every ray. In the second step, we perform an equivariant convolution where the input homogeneous space is a light field, and the output homogeneous space is \mathbb{R}^3 . In the third step, we apply an equivariant transformer on the light field where the key tokens are the rays and the query token is the point for which we want to compute the 3D density.

The reader might wonder why we need three different steps and not, for example, the repetition of an equivariant transformer on input rays colored with the corresponding pixels. The reason we perform the first step of $SE(2)$ convolutions on images is the richness in expressivity in outputs of an $SE(2)$ steerable Resnet. The need for the second step is subtle: an equivariant transformer can have only an equivariant feature as a query representing a 3D point rather than the coordinates of the 3D-point, which would violate the equivariance. To obtain an equivariant feature for the 3D point, we need the second step of light field convolution with outputs on \mathbb{R}^3 .

Throughout the paper, we need the tools to define the signal domains (homogeneous spaces for light field and \mathbb{R}^3) and the associated group actions. Because our features are not composed of scalar channels, we also need the tools from tensor field networks and representation theory.

The main contributions of our work are:

- (1) We propose a novel generalizable reconstruction from multiple views that is equivariant to the frame of reference. The transition from image pixels to 3D densities is accomplished via three equivariant steps.
- (2) We introduce equivariant convolution on light fields for various types of feature fields, and we analytically show how it can be approximated by intra-view spherical convolutions and intra-view $SE(2)$ convolutions.
- (3) To our knowledge, we propose the first equivariant transformer with inputs from a light field and outputs in \mathbb{R}^3 , thus enabling the first equivariant reconstruction from a light field.

2. Related Work

Reconstruction from multiple views Dense reconstruction from multiple views is a well-established field of computer vision with advanced results even before the introduction of deep learning [27]. Such approaches cannot take advantage of shape priors and need a lot of views in order to provide a dense reconstruction. Deep learning enabled semantic reconstruction, namely, the reconstruction from single or multiple views by providing the ground-truth 3D shape during training [15, 44, 73, 74]. These approaches decode the object from a global code without using absolute or relative camera poses. Other works [39, 60, 78] use the camera absolute poses in relation to the object frame or regress the poses using a pretrained pose model [61, 75, 79]. The regression of absolute poses is itself not equivariant and using known poses makes reconstruction not equivariant to camera rotations. There are several prior works [3, 37, 49] that require or predict only the relative poses, however, their structure is not equivariant to camera rotations either.

Light Field The plenoptic function introduced in perception [6] and later in graphics [41] brought a new light into the scene representation problem and was directly applicable to the rendering problem. Instead of reconstructing and then rendering, light fields enabled rendering just by sampling the right rays. Recently, learning-based light field reconstruction [2, 5, 38, 45, 53, 72] became increasingly popular for fronto-parallel novel view synthesis, while [52, 54, 55] combine light field representation with the neural field for the whole outside-in camera setting. Light field networks are more efficient compared to neural radiance fields [46] due to the light field’s smaller dimension. There are only a few studies [11, 42, 52, 54, 64, 80] that concentrate on generalizable rendering. These works are similar to ours in that they obtain the 3D prior from the 2D images, but they are not equivariant because they use conventional attention or convolution or address invariance by view pooling and calculating the variance.

Our paper focuses on 3D reconstruction from a light field. Traditional methods [36, 56, 57, 70] estimate the depth by comparing the correspondence of different views, and [51, 66, 81] extract the depth from the epipolar plane image (EPI). Learning-based methods [32, 33] leverage the 2D CNNs for depth estimation, while [13, 34, 59] make use of attention for feature aggregation. Depth can be estimated by modifying conventional 2D CNNs to be trained for matching cost optimization [65]. None of these approaches defines a light field reconstruction, and none of them is equivariant by design with respect to the choice of frame reference or camera orientations. Our approach achieves this by formally defining a light field convolution that is $SE(3)$ equivariant, and by designing an equivariant pipeline from pixels to 3D densities.

Equivariant Networks In computer vision and machine learning, the equivariant networks are currently being generally investigated, and existing works [12, 17, 18, 20–23, 58, 67, 69, 71] widely apply group convolutional equivariant networks to various types of data and different tasks. Our work is the first to construct group convolutional equivariant networks on the light field.

The convolutional structure over homogeneous space or group is sufficient and necessary for equivariant networks with respect to the compact group are proved in [1, 19, 40]. Recently, [8, 76] provide a uniform way to design the steerable kernel in the equivariant convolutional neural network over homogeneous space through Fourier analysis of the stabilizer group and the whole group, respectively, while [25] use a numerical algorithm to solve the linear constraint of the equivariant map. For arbitrary Lie group, [4, 24, 43] design the uniform group convolutional neural network. The fact that any $O(n)$ equivariant function can be expressed in linear combination with the coefficients as invariant scalars is shown in [62]. For general manifold, [16, 68] derive the general steerable kernel from a differential geometry perspective, where the group convolution over homogeneous space is a special case, and we will also show in the supplemental material for the light field case. Our convolution method is a specific case of [16, 19, 68], however, we are the first to propose the equivariance problem for multi-view reconstruction and apply the group convolution on the light field to address the problem. In the meanwhile, we show how we simplify the equivariant light convolution and propose the $SE(3)$ equivariant transformer model over the light field for 3D reconstruction.

Recently, the equivariant attention models draw increasing attention. [7, 10, 26, 50] combine the attention mechanism with tensor field networks for 3D shape analysis. [47, 48] propose general equivariant self-attention mechanism for arbitrary group, while [35] introduces the equivariant transformer model for Lie groups. We are the first to propose an equivariant transformer (equivariant cross attention model) from light field to 3D Euclidean space.

3. Preliminary

In this work, the light field will be used to construct a 3D equivariant reconstruction. As the light field is the field over the ray space, a homogeneous space of $SE(3)$, we can leverage the generalized equivariant convolutional model proposed in [19]. In the preliminary, we introduce the fundamentals for the mathematical model of feature spaces and the generalized equivariant convolution over homogeneous space in [19].

3.1. Group Actions and Homogeneous Spaces

Given an action of the group G on a homogeneous space X , and given x_0 as the origin of X , the stabilizer group

H of x_0 in G is the group that leaves x_0 intact, i.e., $H = \{h \in G | hx_0 = x_0\}$. The group G can be partitioned into the quotient space (the set of left cosets) G/H and X is isomorphic to G/H since all group elements in the same coset map x_0 to the same element in X , that is, for any element $g' \in gH$ we have $g'x_0 = gx_0$.

Example 1 Take $SE(3)$ as the acting group and the ray space \mathcal{R} as its homogeneous space. We use Plücker coordinates to parameterize the ray space \mathcal{R} : for any $x \in \mathcal{R}$, x can be denoted as (\mathbf{d}, \mathbf{m}) , where $\mathbf{d} \in \mathbb{S}^2$ is the direction of the ray, and $\mathbf{m} = \mathbf{x} \times \mathbf{d}$ where \mathbf{x} is the point on the ray. Then any $g = (R, \mathbf{t}) \in SE(3)$ acts on the ray space as:

$$gx = g(\mathbf{d}, \mathbf{m}) = (R\mathbf{d}, R\mathbf{m} + \mathbf{t} \times (R\mathbf{d})). \quad (1)$$

Given the fixed origin in the homogeneous space as $\eta = ([0, 0, 1]^T, [0, 0, 0]^T)$, the stabilizer group H (the rotation around and translation along the ray) can be parameterized as $H = (R_z(\gamma), t[0, 0, 1]^T)$, i.e., $H \simeq SO(2) \times \mathbb{R}$, and \mathcal{R} is the quotient space G/H up to isomorphism.

Example 2 Consider another case when $SE(3)$ acts on the homogeneous space \mathbb{R}^3 ; for any $g = (R, \mathbf{t}) \in SE(3)$ and $\mathbf{x} \in \mathbb{R}^3$, $g\mathbf{x} = R\mathbf{x} + \mathbf{t}$. If the fixed origin is $[0, 0, 0]^T$, the stabilizer subgroup is $H = SO(3)$ since any rotation $g = (R, \mathbf{0})$ leaves $[0, 0, 0]^T$ unchanged. \mathbb{R}^3 is isomorphic to $SE(3)/SO(3)$.

Example 3 The last example is $SO(3)$ acting on the homogeneous space \mathbb{S}^2 . Given the fixed origin point as $[0, 0, 1]^T$, the stabilizer group is $SO(2)$ and the \mathbb{S}^2 is isomorphic to $SO(3)/SO(2)$.

3.2. Principal Bundle

As stated in [19, 29], the partition of the group G into cosets allows us to treat the group G as the principal bundle where the base space is the homogeneous space G/H ¹, the canonical fiber is the stabilizer group H , the projection map $p : G \rightarrow G/H$ is that $p(g) = gH = gx_0 = x$. The section $s : G/H \rightarrow G$ of p should satisfy that $p \circ s = id_{G/H}$, where $id_{G/H}$ is the identity map on G/H . The action of G causes a twist of the fiber, i.e., $gs(x)$ might not be equal to $s(gx)$ though they are in the same coset, and we use the twist function $h : G \times G/H \rightarrow H$ to denote the twist: $gs(x) = s(gx)h(g, x)$. Same as [19], we simplify $h(g, eH)$ to be $h(g)$, where e is the identity element in G and $eH = x_0$.

Example 4 According to Ex. 2, we can consider a bundle with total space as $SE(3)$, base space as \mathbb{R}^3 , and the fiber as $SO(3)$. For any $g = (R, \mathbf{t}) \in SE(3)$, the projection map

¹We use G/H to denote the homogeneous space since homogeneous space X can be identified with G/H up to isomorphism, i.e., $X \simeq G/H$.

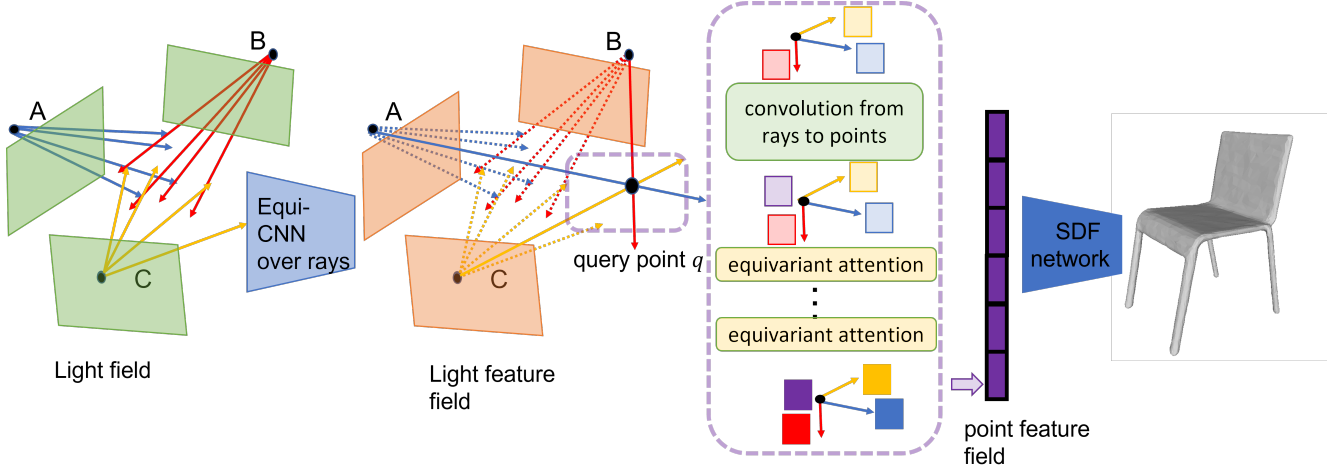


Figure 1. The pipeline of equivariant 3D reconstruction: The first step is to obtain the feature field over the ray space through equivariant spherical CNNs approximated by $SE(2)$ equivariant CNNs. The second step performs a convolution from ray space to point space. The 3rd step applies a transformer in order to obtain a feature for a query through $SE(3)$ equivariant cross attention.

$p : SE(3) \rightarrow \mathbb{R}^3$ projects g as $p(R, \mathbf{t}) = \mathbf{t}$. For any $\mathbf{x} \in \mathbb{R}^3$, the corresponding section map $s : \mathbb{R}^3 \rightarrow SE(3)$ would be: $s(\mathbf{x}) = (R', \mathbf{x})$, where R' is random rotation in $SO(3)$. When we define the section map s as $s(\mathbf{x}) = (I, \mathbf{x})$ for any $\mathbf{x} \in \mathbb{R}^3$, the twist function $h : SE(3) \times \mathbb{R}^3 \rightarrow SO(3)$ is that $h(g, \mathbf{x}) = s(gx)^{-1}gs(\mathbf{x}) = R$ for any $\mathbf{x} \in \mathbb{R}^3$ and any $g = (R, \mathbf{t}) \in SE(3)$. This twist function is independent of \mathbf{x} due to the fact that $SE(3) = \mathbb{R}^3 \rtimes SO(3)$ is a semidirect product group as stated in [19].

Example 5 As shown in Ex. 3, $SO(3)$ can be viewed as a principal bundle with the base space as \mathbb{S}^2 and the fiber as $SO(2)$. With the rotation $R \in SO(3)$ parameterized as $R = R_Z(\alpha)R_Y(\beta)R_Z(\gamma)$, the projection map $p : G \rightarrow G/H$ maps R in such way:

$$\begin{aligned} p(R) &= R_Z(\alpha)R_Y(\beta)R_Z(\gamma)[0, 0, 1]^T \\ &= R_Z(\alpha)R_Y(\beta)[0, 0, 1]^T \\ &= [\sin(\beta)\cos(\alpha), \sin(\beta)\sin(\alpha), \cos(\beta)]^T. \end{aligned}$$

For any $\mathbf{d} \in \mathbb{S}^2$, the section map $s : \mathbb{S}^2 \rightarrow SO(3)$ of p should satisfy that $s(\mathbf{d})[0, 0, 1]^T = \mathbf{d}$, for instance, the section map s could be:

$$s(\mathbf{d}) = R_Z(\alpha_{\mathbf{d}})R_Y(\beta_{\mathbf{d}}),$$

where $\alpha_{\mathbf{d}}$ and $\beta_{\mathbf{d}}$ satisfies that

$$\mathbf{d} = [\sin(\beta_{\mathbf{d}})\cos(\alpha_{\mathbf{d}}), \sin(\beta_{\mathbf{d}})\sin(\alpha_{\mathbf{d}}), \cos(\beta_{\mathbf{d}})]^T.$$

As defined, the twist function $h : SO(3) \times \mathbb{S}^2 \rightarrow SO(2)$ is that $h(R, \mathbf{d}) = s(R\mathbf{d})^{-1}Rs(\mathbf{d})$.

Example 6 The final example is $SE(3)$ with \mathbb{R} as the base space and $SO(2) \times \mathbb{R}$ as the fiber, which is the focus of this

work, as shown in figure 2. According to the group action defined in Eq.1, the projection map $p : SE(3) \rightarrow \mathcal{R}$ is:

$$p(R, \mathbf{t}) = (R, \mathbf{t})\eta = (R[0, 0, 1]^T, \mathbf{t} \times (R[0, 0, 1]^T))$$

that represents a ray direction with the 3rd column of a rotation matrix and the \mathbf{m} Plücker as its cross product with the translation. we show here how to construct a section $s : G/H \rightarrow G$ using the Plücker coordinates:

$$s((\mathbf{d}, \mathbf{m})) = (s_a(\mathbf{d}), s_b(\mathbf{d}, \mathbf{m})),$$

where $s_a(\mathbf{d}) \in SO(3)$ can be any rotation that $s_a(\mathbf{d})[0, 0, 1]^T = \mathbf{d}$, a section map from \mathbb{S}^2 to $SO(3)$ as shown in Ex. 5; and $s_b(\mathbf{d}, \mathbf{m}) \in \mathbb{R}^3$ can be any point on the ray (\mathbf{d}, \mathbf{m}) . For example the section map could be $s((\mathbf{d}, \mathbf{m})) = (R_Z(\alpha_{\mathbf{d}})R_Y(\beta_{\mathbf{d}}), \mathbf{d} \times \mathbf{m})$, where $\alpha_{\mathbf{d}}$ and $\beta_{\mathbf{d}}$ satisfy that $\mathbf{d} = R_Z(\alpha_{\mathbf{d}})R_Y(\beta_{\mathbf{d}})[0, 0, 1]^T$.

Given the section map, for any $g = (R_g, \mathbf{t}_g) \in SE(3)$ and $x = (\mathbf{d}_x, \mathbf{m}_x) \in \mathcal{R}$, we define the twist function $h : SE(3) \times \mathcal{R} \rightarrow SO(2) \times \mathbb{R}$ is $h(g, x) = s^{-1}(gx)gs(x) = (h_a(R_g, \mathbf{d}_x), h_b(R, x))$, where $h_a : SO(3) \times \mathbb{S}^2 \rightarrow SO(2)$ is the twist function corresponding to s_a , as shown in Ex. 5, and $h_b(g, x) = \langle R_g s_b(x) + \mathbf{t}_g - s_b(gx), R_g \mathbf{d}_x \rangle [0, 0, 1]^T$. In the case of above example section s , the twist function $h : SE(3) \times \mathcal{R} \rightarrow SO(2) \times \mathbb{R}$ is

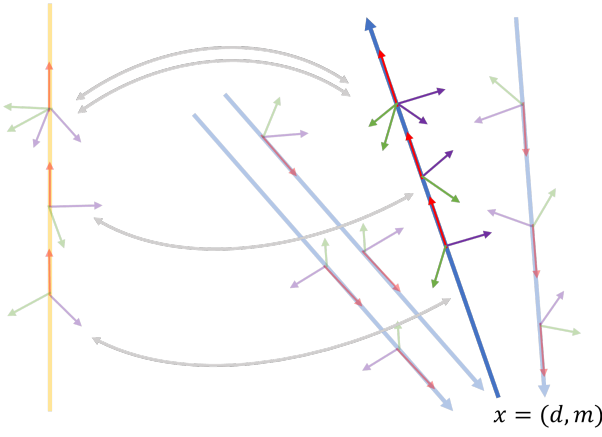
$$h(g, x) = s^{-1}(gx)gs(x) = (R_Z(R_g, \mathbf{d}_x), \langle \mathbf{t}_g, (R_g \mathbf{d}_x) \rangle [0, 0, 1]^T),$$

$$\text{where } R_Z(R_g, \mathbf{d}_x) = R_Y^{-1}(\beta_{R_g} \mathbf{d}_x) R_Z^{-1}(\alpha_{R_g} \mathbf{d}_x) R_g R_Z(\alpha_{R_g} \mathbf{d}_x) R_Y(\beta_{R_g} \mathbf{d}_x).$$

3.3. Associated Vector Bundle

Given the principal bundle G , we can construct the associated vector bundle by replacing the fiber H with the vector

$$p^{-1}(x) \simeq SO(2) \times \mathbb{R}$$



$$H = SO(2) \times \mathbb{R}$$

Figure 2. We can view $SE(3)$ as a $SO(2) \times \mathbb{R}$ -principal bundle, where the projection map $p : SE(3) \rightarrow \mathcal{R}$ is $p(R, t) = (R[0, 0, 1]^T, t \times (R[0, 0, 1]^T))$, and the inverse of p is that $p^{-1}(x) = \{(R, t) | (R, t)\eta = x\}$. The coordinate frames denote elements in $SE(3)$. For one ray $x = (\mathbf{d}, \mathbf{m})$ (illustrated as the blue ray), then the coordinate frames on the ray with Z -axis aligning with the ray x are in $p^{-1}(x)$. As shown in the figure, $p^{-1}(x)$ isomorphic to $H = SO(2) \times \mathbb{R}$.

space V , where $V \simeq \mathbb{R}^n$ and H acts on V through a group representation $\rho : G \rightarrow GL(V)$. The group representation corresponds to the type of geometric quantity in the vector space V , for example, the scalar, the vector, or the higher-order tensor.

We can obtain a quotient space $E = G \times_{\rho} V/H$ through defining the right action of H on $G \times V$: $(g, v)h = (gh, \rho(h)^{-1}v)$ for any $h \in H$, $g \in G$ and $v \in V$. With the defined projection map $p : G \times_{\rho} V \rightarrow G/H$: $p([g, v]) = gH$, where $[g, v] = \{(gh, \rho(h^{-1})v) | h \in H\}$, the element in $G \times_{\rho} V$, we get the fibre bundle E associated to the principal bundle G .

The feature function $f : G/H \rightarrow V$ can encode the section of the associated vector bundle $s_v : G/H \rightarrow G \times_{\rho} V$: $s_v(x) = ([s(x), f(x)])$, where s is the section map of the principal bundle as defined in Sec. 3.2. The group G acting on the field f as shown in [19]:

$$(\mathcal{L}_g f)(x) = \rho(h(g^{-1}, x))^{-1} f(g^{-1}x), \quad (2)$$

where $h : G \times G/H \rightarrow H$ is the twist function as defined in Sec. 3.2.

3.4. Equivariant Convolution Over Homogeneous Space

The generalized equivariant convolution over homogeneous space, as stated in [19], that maps a feature field $f^{l_{in}}$

over homogeneous space G/H to a feature $f^{l_{out}}$ over homogeneous space G/H by convolving with a kernel κ is defined as:

$$f^{l_{out}}(x) = \int_{G/H} \kappa(s(x)^{-1}y) \rho_{in}(h(s(x)^{-1}s(y))) f^{l_{in}}(y) dy \quad (3)$$

where ρ_{in} is the group representation of H_1 corresponding to the feature type l_{in} ², s is the section map (see Sec. 3.2), h is the twist function (see Sec. 3.2).

The convolution is equivariant with respect to G , that is

$$\mathcal{L}_g^{out} f^{l_{out}} = \kappa * \mathcal{L}_g^{in} f^{l_{in}},$$

if and only if $\kappa(hx) = \rho_{out}(h)\kappa(x)\rho_{in}(h^{-1}(h, x))$, where ρ_{in} and ρ_{out} are the group representations of H corresponding to the feature type l_{in} and l_{out} , respectively.

Example 7 Take $SE(3)$ -equivariant convolution over \mathbb{R}^3 as an example. If we use the section map as stated in Ex. 4, we will find that $h(s(x)^{-1}s(y)) = (I, \mathbf{0})$, therefore convolution 3 becomes:

$$\begin{aligned} f^{l_{out}}(x) &= \int_{G/H} \kappa(s(x)^{-1}y) f^{l_{in}}(y) dy \\ &= \int_{G/H} \kappa(y - x) f^{l_{in}}(y) dy \end{aligned}$$

and κ should satisfy

$$\begin{aligned} \kappa(Rx) &= \rho_{out}(R)\kappa(x)\rho_{in}(h^{-1}(R)) \\ &= \rho_{out}(R)\kappa(x)\rho_{in}^{-1}(R) \\ &= D_{l_{out}}(R)\kappa(x)D_{l_{in}}(R)^{-1} \end{aligned}$$

for any $R \in SO(3)$, where $D^{l_{in}}$ and $D^{l_{out}}$ are the Wigner-D matrices, i.e. irreducible representations corresponding to the feature types l_{in} and l_{out} , which is the same as the analytical result in [69].

Example 8 For spherical convolution, the convolution integral becomes:

$$\begin{aligned} f^{l_{out}}(\alpha, \beta) &= \int_{\alpha' \in [0, 2\pi], \beta' \in [0, \pi]} \kappa(R_Y^{-1}(\beta)R_Z^{-1}(\alpha)R_Z(\alpha')R_Y(\beta')\eta) \\ &\quad \rho_{in}(h(R_Y^{-1}(\beta)R_Z^{-1}(\alpha)R_Z(\alpha')R_Y(\beta'))f^{l_{in}}(\alpha', \beta')d\alpha' \sin(\beta')d\beta' \end{aligned}$$

where $\eta \in [0, 0, 1]^T$ is the fixed original point as stated in Ex. 3, ρ_{in} is the group representation of $SO(2)$ corresponding to the feature type l_{in} , in this case, $\rho_{in}(\theta) =$

²Here we use the feature type to denote the type of geometric quantity in vector space V_{in} or V_{out} .

$e^{-il_{in}\theta}$. The kernel κ should satisfy that $\kappa(R(\theta)x) = e^{-il_{out}\theta}xe^{il_{in}\theta}$ for any $R(\theta) \in SO(2)$.

Specifically, when the input and output are scalar feature fields over the sphere, convolution reads

$$\begin{aligned} f^{out}(\alpha, \beta) &= \int_{\alpha' \in [0, 2\pi), \beta' \in [0, \pi)} \kappa(R_Y^{-1}(\beta)R_Z^{-1}(\alpha)R_Z(\alpha')R_Y(\beta')\eta) \\ &\quad f^{in}(\alpha', \beta')d\alpha' \sin(\beta')d\beta' \end{aligned}$$

κ has such constraint:

$$\kappa(R(\theta)x) = \kappa(x)$$

for any $R(\theta) \in SO(2)$, which enable us define $\kappa'(g\eta) = \kappa(g^{-1}\eta)$. We have $\kappa'(R(\theta)x) = \kappa'(x)$ for any $R(\theta) \in SO(2)$, and it is consistent with the convolution in [21] where κ' is the convolution kernel in [21].

Example 9 In our case, the equivariant convolution over the ray space is also based on the generalized equivariant convolution over a homogeneous space. See 4.1 for the details.

4. Method

We start by defining what an $SE(3)$ -equivariant reconstruction from a light field is, and how it is related to an equivariant reconstruction from multiple views. We use $\mathcal{F} = \{f : \mathcal{R} \rightarrow \mathbb{R}\}$ to denote a light field mapping from ray space to scalars, and $\mathcal{E} = \{e : \mathbb{R}^3 \rightarrow \mathbb{R}\}$ to denote a signed distance field (SDF).

A 3D reconstruction $\Phi : \mathcal{F} \rightarrow \mathcal{E}$ is equivariant when for any $g \in SE(3)$ and any $x \in \mathbb{R}^3$,

$$\Phi(\mathcal{L}_g f)(x) = \mathcal{L}'_g(\Phi(f))(x),$$

where \mathcal{L}_g and \mathcal{L}'_g are group actions on the light field and the SDF, respectively. Specifically, for any $f \in \mathcal{F}$, $x \in \mathcal{R}$, $g \in SE(3)$, $(\mathcal{L}_g f)(x) = f(g^{-1}x)$, and for any $e \in \mathcal{E}$, $x \in \mathbb{R}^3$, $g \in SE(3)$, $(\mathcal{L}'_g e)(x) = e(g^{-1}x)$.

In practice, we have a finite sampling of the light field corresponding to the pixels of multiple views $\mathcal{V} = \{V : V = \{v_1, v_2, \dots, v_n\}\}$. The 3D reconstruction Φ is equivariant when for any $g \in SE(3)$ and any $x \in \mathbb{R}^3$:

$$\Phi(g \cdot V)(x) = \mathcal{L}'_g(V)(x).$$

If we denote V as (L_V, f) , where L_V is the set of rays in V and f is the light field induced by multi views v_1, v_2, \dots, v_n sample from, then $g \cdot V = (g \cdot L_V, \mathcal{L}_g f)$, where $g \cdot L_V$ is g acting on the rays as defined Eq.1.

We achieve equivariance using three steps as illustrated in Fig. 1: (1) the transition from pixel colors to a feature-valued light field (equi-CNN over rays), (2) the computation

of features in \mathbb{R}^3 from features on the ray space \mathcal{R} , and (3) the equivariant attention/transformer with the query being a feature on the point we want to compute SDF and key/value being features on rays.

4.1. Equivariant Convolution over Rays

As stated in 3.3, given the section map of the principal $SO(2) \times \mathbb{R}$ -bundle $SE(3)$, the features $f : \mathcal{R} \rightarrow \mathbb{R}^l$ can encode fields on the ray space, the section of the associated vector bundle $SE(3) \times_{\rho} \mathbb{R}^l$, and $g \in G$ acts on the field as Eq. 2, where ρ is the group representation of $SO(2) \times \mathbb{R}$ corresponding to the field type of f . Since $H = SO(2) \times \mathbb{R}$ is a product group, for any $h = (\gamma, t)$, $\rho(\gamma, t) = \rho_1(\gamma) \otimes \rho_2(t)$, where ρ_1 is the group representation of $SO(2)$ and ρ_2 is the group representation of \mathbb{R} . The convolution is equivariant with respect to $SE(3)$ only and if only $\kappa(hx) = \rho_{out}(h)\kappa(x)\rho_{in}(h^{-1}(h, x))$, where ρ_{in} and ρ_{out} are the group representations of $SO(2) \times \mathbb{R}$ corresponding to the input feature type l_{in} and output feature type l_{out} , respectively.

Although the aforementioned convolution is defined on the whole continuous ray space, in practice, we have multiple views. However, the equivariance still strictly stands when the ray sampling (pixels from camera views) is the same up to coordinate change. We will next explain how we will convert the light field convolution to an intra-view $SE(2)$ -convolution.

Local kernel support The equivariance stands even if we constrain the kernel to be local. When $x = (\mathbf{d}_x, \mathbf{m}_x)$ meets the condition that $\angle(\mathbf{d}_x, [0, 0, 1]^T) \leq \beta_0$ and $\|\mathbf{m}_x\| \leq d_0$, $\kappa(x) \neq 0$, this local support will not break the constraint that $\kappa(hx) = \rho_{out}(h)\kappa(x)\rho_{in}(h^{-1}(h, x))$. Then, convolution in Eq. 3 is accomplished over the neighbors only as visualized in Fig. 3.

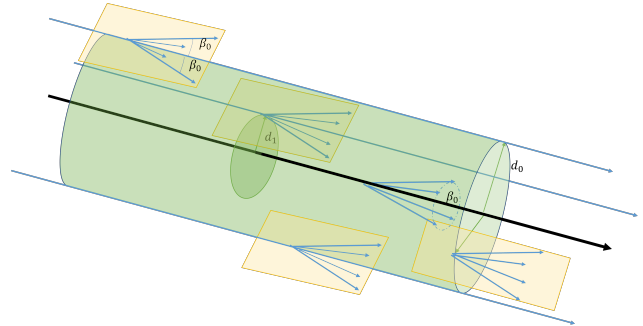


Figure 3. Any ray $y = (\mathbf{d}_y, \mathbf{m}_y)$ (denoted in blue) in the neighboring ray set of a ray $x = (\mathbf{d}_x, \mathbf{m}_x)$ will go through the cylinder with x as the axis and d_0 as the radius since $d(x, y) \leq d_0$. Moreover, for any y , $\angle(\mathbf{d}_y, \mathbf{d}_x) \leq \beta_0$. Actually, any ray $y \in \mathcal{N}(x)$ is on one tangent plane of a cylinder with x as the axis and $d(x, y)$ as the radius when $d(x, y) > 0$.

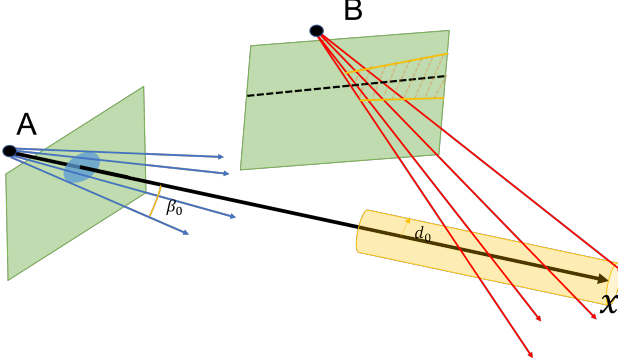


Figure 4. For a ray x from view A, one part of the neighboring rays are from view A, as noted by the blue rays; the other part are from the other view B, as noted by the red rays. The neighboring rays from view B are neighboring pixels, noted by the yellow part in view B, of the epipolar line view B corresponding to ray x in view A, noted by the black dashed line. The yellow part pixels are not traversed because of the angle constraint of the kernel.

From light field to intra-view convolution Following Fig. 4, neighboring rays are composed of two parts: a set of rays from the same view and another set of rays from different views. For one ray x in view A, the neighboring rays from view B are in the neighborhood of the epipolar line of x in view B. When the two views are close to each other, the neighborhood in the view B would be very large. If we consider the equivariance kernel constraint $\kappa(hx) = \rho_{out}(h)\kappa(x)\rho_{in}(h^{-1}(h,x))$, the fact that $\angle(\mathbf{d}_x, [0, 0, 1]^T)$ and $d((x, [0, 0, 1]^T)$ remain unchanged when $h \in SO(2) \times \mathbb{R}$ acts on x suggests that $\kappa(x)$ is related to $\angle(\mathbf{d}_x, [0, 0, 1]^T)$ and $d((x, [0, 0, 1]^T)$. It would be memory- and time-consuming to memorize the two metrics beforehand or to compute the angles and distances on the fly. Practically, the light field is only sampled from a few sparse viewpoints, which causes the relative angles of the rays in different views to be large and allows them to be excluded from the kernel neighborhood. As a result, in our implementation, the ray neighborhood is composed of only rays in the same view.

From intra-view light field to spherical convolution After showing that a small kernel support in the case of sparse views affects only intra-view rays, we will prove here that an intra-view light-field convolution is equivalent to a spherical convolution. We will exploit the fact that a feature defined on a ray is constant along the ray. This means that the translation part of the stabilizer group (translation along the ray) leaves the feature as is. In math terms, the irreducible representation for the translation \mathbb{R} is the identity, which means that the field function is a scalar field for the translation group, with the formula $(\mathcal{L}_t f)(x) = f(t^{-1}x)$. The equivariant condition on the kernel can then be simplified as

$$\kappa((h, t)x) = \rho_{out}(h)\kappa(x)\rho_{in}(h_a^{-1}(h, \mathbf{d}_x)),$$

where $h \in SO(2)$ and $t \in \mathbb{R}$, ρ_{in} and ρ_{out} are irreducible representations for $SO(2)$, and h_a is the twist function we define above that $h(g, x) = (h_a(R_g, \mathbf{d}_x), h_b(g, x))$, i.e., the twist of the fiber introduced by action of $SO(3)$ as shown in Ex. 5.

Now we describe the relationship between the intra-view light-field convolution and the spherical convolution:

Proposition 4.1 *If the translation group acts on feature $f : \mathcal{R} \rightarrow V$ as $(\mathcal{L}_t f)(x) = f(t^{-1}x)$ for any $x \in \mathcal{R}$, the equivariant intra-view light-field convolution:*

$$f^{l_{out}}(x) = \int_{y \in \mathcal{N}(x)} \kappa(s(x)^{-1}y)\rho_{in}(h(s(x)^{-1}s(y)))f^{l_{in}}(y)dy$$

becomes a spherical convolution:

$$\begin{aligned} f^{l_{out}}(x) &= \int_{\mathbf{d}_y \in \mathbb{S}^2} \kappa'(s_a(\mathbf{d}(x))^{-1}\mathbf{d}_y)\rho_{in}(h_a(s_a(\mathbf{d}_x)^{-1}s_a(\mathbf{d}_y))) \\ &f'^{l_{in}}(\mathbf{d}_y)d\mathbf{d}_y, \end{aligned} \quad (4)$$

where $f'^{l_{in}}(\mathbf{d}_y) = f^{l_{in}}(\mathbf{d}_y, \mathbf{c}_x \times \mathbf{d}_y)$, \mathbf{c}_x denotes the camera center that x goes through, and $\kappa'(s_a(\mathbf{d}_x)^{-1}\mathbf{d}_y) = \kappa(s_a(\mathbf{d}_x)^{-1}\mathbf{d}_y, (s(x)^{-1}\mathbf{c}_x) \times (s_a(\mathbf{d}_x)^{-1}\mathbf{d}_y))$.

See supplemental material Sec. A for the proof. The rough idea is that we can replace $f'^{l_{in}}(\mathbf{d}_y, \mathbf{c}_x \times \mathbf{d}_y)$ with $f'^{l_{in}}(\mathbf{d}_y)$ because any ray $y \in \mathcal{N}(x)$ goes through \mathbf{c}_x and \mathbf{c}_x is fixed for any view. The reason we can construct κ' in the above way is that for any $t \in \mathbb{R}$, according to the derived simplified equivariant kernel condition $\kappa((e, t)x) = \kappa(x)$, where e is the identity element in $SO(2)$. Then when $t = ((-s(x)^{-1}\mathbf{c}_x))^T[0, 0, 1]^T$, we have $\kappa(s_a(x)^{-1}\mathbf{d}_y, s(x)^{-1}\mathbf{c}_x \times (s_a(x)^{-1}\mathbf{d}_y)) = \kappa((s_a(x)^{-1}\mathbf{d}_y, [0, 0, 0]^T))$. Eq. 4 shows that it is exactly the spherical convolution with features of different types [22, 76] individually for every set of rays in the same view. Therefore convolution 3 is equivariant to the independent rotations of the camera.

From SO(3)- to SE(2)-convolution While there is an established framework for spherical convolution using a Fourier transform [18, 21, 22] it is not applicable in our case because the boundaries of the constrained field of view cause an explosion in the high frequencies of the spherical harmonics. We will make a compromise here and approximate the SO(3) convolution with an SE(2) convolution on the image plane by making the assumption that the field of view is small. One can see the rationale behind this approximation by keeping only the first order terms in the optical flow equation: the rotational term is only due to Ω_z

while the translational term is $(-T_x - \Omega_y, -T_y + \Omega_x)$ with $(\Omega_x, \Omega_y, \Omega_z)$ as the angular velocity. We provide a justification using the formalism of the previous paragraphs in the supplemental material Sec. C.

4.2. Equivariant convolution from light field to points

We use an implicit function for reconstruction (SDF) defined on \mathbb{R}^3 that is also a homogeneous space of $SE(3)$ like the ray space \mathcal{R} . Using a convolution we will define an equivariant map between fields on these two homogeneous spaces. We denote with H_1 and H_2 the stabilizer groups corresponding to the input and output homogeneous spaces, respectively, i.e. $SO(2) \times \mathbb{R}$ and $SO(3)$.

As shown in Ex. 4, We can choose the section map $s_2 : \mathbb{R}^3 \rightarrow SE(3)$: $s_2(t) = (I, t)$ for any $t \in \mathbb{R}^3$ and I is the identity matrix.

In this convolution, the input feature field f_1^{in} defined on the light field is of scalar type. Following [19], convolution becomes:

$$f_2^{l_{out}}(x) = \int_{G/H_1} \kappa(s_2(x)^{-1}y) f_1^{in}(y) dy, \quad (5)$$

where $h_2 \in H_2$, $\kappa(h_2x) = \rho_{out}(h_2)\kappa(x)$, and ρ_{out} is the irreducible representation of H_2 corresponding to the feature type l_{out} . The subscripts of the input feature and output feature denote the homogeneous spaces they are defined on.

We can derive $\kappa(h_2x) = \rho_{out}(h_2)\kappa(x)$ analytically: for any $x = (\mathbf{d}_x, \mathbf{m}_x) \in L$, if $\|\mathbf{m}_x\| = 0$, $\kappa(x) = c Y^{l_{out}}(\mathbf{d}_x)$, where c is an arbitrary constant and $Y^{l_{out}}$ is the spherical harmonics and l_{out} is the order (type) of output tensor; With $\|\mathbf{m}_x\| \neq 0$, $\kappa(x)$ becomes $\rho_{out}(\hat{x})f(\|\mathbf{m}_x\|_x)$, where \hat{x} denotes the element $(\mathbf{d}_x, \frac{\mathbf{m}_x}{\|\mathbf{m}_x\|}, \mathbf{d}_x \times \frac{\mathbf{m}_x}{\|\mathbf{m}_x\|})$ in $SO(3)$ and $f : \mathbb{R} \rightarrow \mathbb{R}^{(2l_{out}+1) \times 1}$.

In the experiments, we found that $d_0 = 0$ achieves the best performance, meaning the neighborhood only includes the rays from all views going through the point. Hence, we can simplify the convolution to

$$f_2^{l_{out}}(x) = \int_{d(y,x)=0} Y^{l_{out}}(\mathbf{d}_{s_2(x)^{-1}y}) \text{MLP}(f_1^{in}(y)) dy,$$

In fact, this equation shows that for every point x , we can treat the ray y going through x with feature f_1^{in} as a point y' , where $y' - x = \mathbf{d}_{s_2(x)^{-1}y}$ as shown in figure 5, with the scalar feature f_1^{in} . Moreover, in the implementation of convolution, we can concatenate the feature f_1^{in} with the embedding of point x 's depth, which will break the ideal equivariance for continuous light field theoretically, but will not break the equivariance in practice since rarely two cameras will share one ray. The equivariant convolution becomes then

$$f_2^{l_{out}}(x) = \int_{d(y,x)=0} Y^{l_{out}}(\mathbf{d}_{s_2(x)^{-1}y}) \text{MLP}(f_1^{in}(y) \| \|x - \mathbf{c}_y\|) dy$$

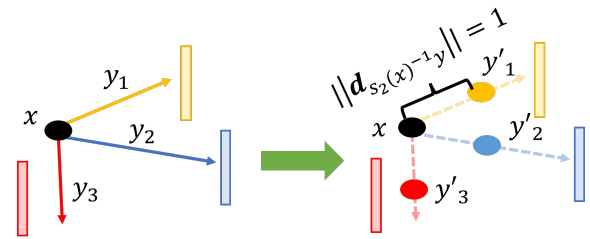


Figure 5. Interpreting rays y_i as points y'_i

where \mathbf{c}_y denotes the camera center of the ray y .

4.3. Equivariant Light Field Transformer

For the third step, we introduce an equivariant transformer in order to alleviate the loss of expressivity due to the isotropic kernel κ in Eq. 5. Again here, the attention key and values are from ray space while the query is from \mathbb{R}^3 .

The equivariant transformer in general form is:

$$f_2^{out}(x) = \sum_{y \in \mathcal{N}(x)} \frac{\exp(\langle f_q(x, f_2^{in}), f_k(x, y, f_1^{in}) \rangle)}{\sum_{y \in \mathcal{N}(x)} \exp(\langle f_q(x, f_2^{in}) f_k(x, y, f_1^{in}) \rangle)} f_v(x, y, f_1^{in}) \quad (6)$$

where f_2^{out} is the output feature, f_2^{in} is the input feature associated with the query point and f_1^{in} is the input feature associated with the ray.

Noted that f_2^{out} , f_2^{in} and f_1^{in} are features that are composed of fields of different types, denoted as $f_2^{out} = \oplus_i f_2^{l_{out_i}}$, $f_2^{in} = \oplus_i f_2^{l_{in_i}}$, and $f_1^{in} = \oplus_i f_1^{l_{in_i}}$ ³. f_k , f_q , and f_v are constructed equivariant key features, query features, and value features, respectively, which are composed of fields of different types as well. The types of fields in f_k and f_q should be the same since we need to compute an inner product for each type of feature to get the invariant attention weights. We use $f_k = \oplus_i f_k^{l_{ki}}$, $f_q = \oplus_i f_q^{l_{ki}}$, and $f_v = \oplus_i f_v^{l_{vi}}$ to denote f_k , f_q and f_v , respectively.

We construct the features f_k , f_q and f_v through the equivariant kernels $\kappa_k = \oplus_{j,i} \kappa_k^{l_{kj}, l_{in_i}}$, $\kappa_v = \oplus_{j,i} \kappa_v^{l_{vj}, l_{in_i}}$ and

³Since here the homogeneous spaces of input and output are different, so as the stabilizer groups, we use l and l' to denote the irreducible representations of different stabilizer groups.

equivariant matrix $W_q = \bigoplus_{j,i} W_q^{l_{k_j}, l_{in_i}}$:

$$\begin{aligned} f_k^{l_{k_j}}(x, y, f_1^{in}) &= \sum_i \kappa_k^{l_{k_j}, l'_{in_i}} (s_2(x)^{-1} y) \rho_1^{l'_{in_i}} (\mathbf{h}_1(s_2(x)^{-1} s_1(y))) f_1^{l'_{in_i}}(y); \\ f_q^{l_{k_j}}(x, f_2^{in}) &= \sum_i W_q^{l_{k_j}, l_{in_i}} f_2^{l_{in_i}}(x); \\ f_v^{l_{v_j}}(x, y, f_1^{in}) &= \sum_i \kappa_v^{l_{v_j}, l'_{in_i}} (s_2(x)^{-1} y) \rho_1^{l'_{in_i}} (\mathbf{h}_1(s_2(x)^{-1} s_1(y))) f_1^{l'_{in_i}}(y), \end{aligned}$$

where for any i, j , any $h_2 \in SO(3)$, and any $x \in \mathcal{R}$, $\kappa_k^{l_{k_j}, l'_{in_i}}$ and $\kappa_v^{l_{v_j}, l'_{in_i}}$ should satisfy that:

$$\begin{aligned} \kappa_k^{l_{k_j}, l'_{in_i}}(h_2 x) &= \rho_2^{l_{k_j}}(h_2) \kappa_k^{l_{k_j}, l'_{in_i}}(x) \rho_1^{l'_{in_i}}(\mathbf{h}_1^{-1}(h_2, x)); \\ \kappa_k^{l_{v_j}, l'_{in_i}}(h_2 x) &= \rho_2^{l_{v_j}}(h_2) \kappa_v^{l_{v_j}, l'_{in_i}}(x) \rho_1^{l'_{in_i}}(\mathbf{h}_1^{-1}(h_2, x)), \end{aligned}$$

where $\mathbf{h}_1(h_2, x) = s_1(h_2 x)^{-1} h_2 s_1(x)$ is the twist function, and for any i, j and any $h_2 \in SO(3)$, $W_q^{l_{k_j}, l_{in_i}}$ satisfies that:

$$\rho_2^{l_{k_j}}(h_2) W_q^{l_{k_j}, l_{in_i}} = W_q^{l_{k_j}, l_{in_i}} \rho_1^{l_{in_i}}(h_2).$$

Due to Schur's Lemma, we have $W_q^{l_{k_j}, l_{in_i}} = cI$ when $l_{k_j} = l_{in_i}$, where c is an arbitrary real number, otherwise $W_q^{l_{k_j}, l_{in_i}} = \mathbf{0}$.

With the aforementioned construction, we consequently claim the following in this work:

Proposition 4.2 *The transformer as shown in the equation 6 from the ray space to \mathbb{R}^3 is $SE(3)$ equivariant.*

See the supplementary material Sec. D for proof.

In the implementation, we apply a transformer over the rays going through the query point. We can continue to use the interpretation in the convolution from ray space to \mathbb{R}^3 that treats any ray y passing through the point x as a point y' such that $y' - x = \mathbf{d}_{s_2(x)^{-1} y}$. After we get the initial feature of query points through equivariant convolution from \mathcal{R} to \mathbb{R}^3 , we update the neighboring ray feature by directly concatenating the query point feature to every ray feature before through a $SO(3)$ equivariant MLP as shown in the figure 6. $SO(3)$ equivariant MLP is composed of equivariant nonlinear layers and self-interaction layers as in the tensor field networks [58].

Since y becomes point y' , and f_1^{in} is the feature over \mathbb{R}^3 attached to "points" y' , it becomes $\bigoplus_i f_1^{l_{in_i}}$. Then transformer in the equation 6 would be converted to the transformer in [26] over \mathbb{R}^3 . The details are shown in the supplementary material Sec. E.

⁴Since here f_1^{in} is the fields over \mathbb{R}^3 , we use l instead of l' as the denotation

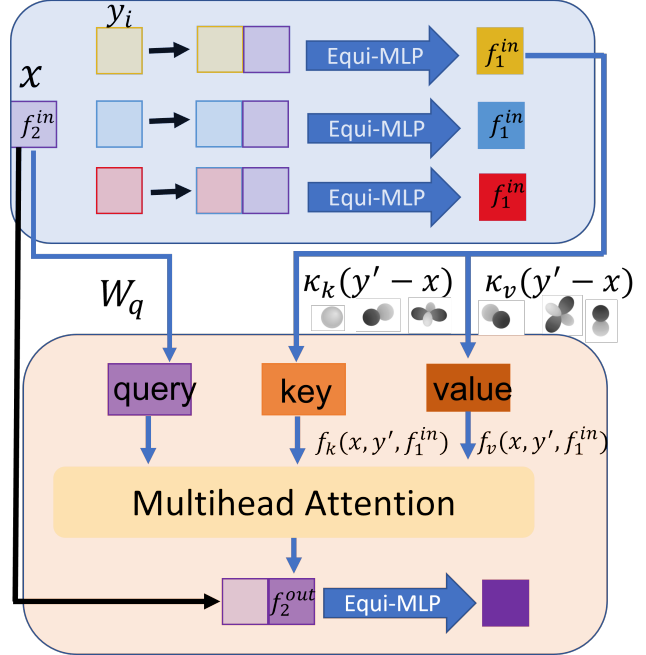


Figure 6. The structure of ray updating and $SE(3)$ transformer. We treat any ray y going through point x as a point $y' \in \mathbb{R}^3$ such that $y' - x = \mathbf{d}_{s_2(x)^{-1} y}$. The blue block indicates the ray feature update, and the pink block is the equivariant attention model. For the ray feature updating, the point feature (lavender) is concatenated to every ray feature (light yellow, light blue, and light red), which is the direct sum of features with various types. For the transformer part, we get the query, key, and value feature through the equivariant linear map and apply multi-head attention to obtain the output point feature.

5. Experiment

We use the same train/val/test split of the Shapenet Dataset [9] and render ourselves for the equivariance test. In order to render the views for each camera, we fix eight cameras to one cube's eight corners. The cameras all point in the same direction toward the object's center. We produce five datasets called I, Z, R, Y, $SO(3)$, depending on the orientations of the cameras and the orientation of the object, respectively.

The I dataset is obtained by fixing the orientation of the object as well as the eight camera orientations.

With the object orientation fixed, we can independently rotate each camera around its optical axis by a random angle in a uniform distribution of $(-\pi, \pi]$ to obtain the Z dataset. For the R dataset, we rotate every camera randomly by any rotation in $SO(3)$ while fixing the object. As stated in Sec. 3.1, the equivariance stands with the content unchanged. Therefore in practice, we require that the object projection after the rotation does not have new parts of the object. We satisfy this assumption by forcing the camera to fixate on a

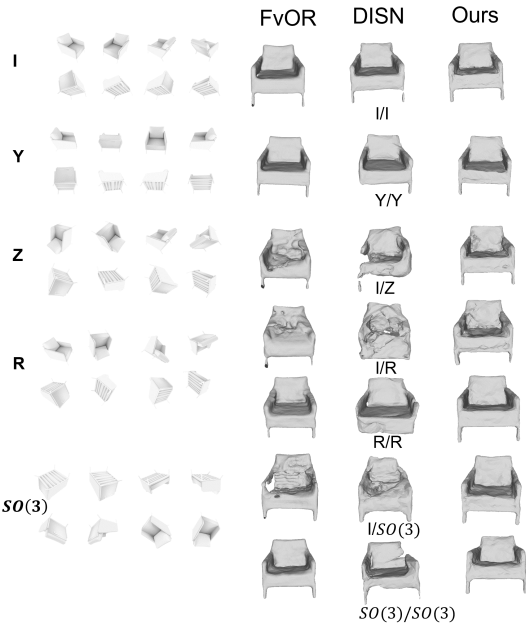


Figure 7. Qualitative results for equivariant reconstruction. The left part is the views, and the right part is the reconstruction meshes of different models. The captions below the meshes show how the model is trained and tested.

new random point inside a small neighborhood and subsequently rotate each camera around its optical axis with the uniformly random angle in $(-\pi, \pi]$.

We generate the Y dataset by rotating the object only with azimuthal rotations while keeping the camera orientations the same.

The $SO(3)$ dataset is generated by rotating the object with random rotation in $SO(3)$ with the orientations of cameras unchanged, which will potentially result in new image content. Equivariance is not theoretically guaranteed in this setup, but we still want to test the performance of our method.

Implementation Details As described in Sec 3.2, we use $SE(2)$ equivariant CNNs to approximate the equivariant convolution over the rays. We use the same ResNet backbone as implemented in [31] that is equivariant to the finite group C_8 , which we find achieves the best result compared with other $SE(2)$ equivariant CNNs. We use a similar pyramid structure as [75] that concatenates the output feature of every block. Since every hidden feature is the regular representation, we use 1×1 $SE(2)$ -equivariant convolutional layers to transfer the hidden representation to scalar type.

For the fusion from the ray space to the point space model, we use one layer of convolution and three combined blocks of updating ray features and $SE(3)$ transformers.

For the equivariant $SE(3)$ multi-head-attention, we only use the scalar feature and the vector (type-1) feature in the hidden layer. The kernel matrix includes the spherical harmonics of degree-0 and degree-1. We also concatenate every output point feature of every block as in the $2D$ backbone. Since the output feature of every block includes the vector feature, we transfer it to the scalar feature through one vector neuron layer and the inner vector product.

We use the same training loss as in [75], which applies both uniform and near-surface sampling during training, and leverage the weighted SDF loss for sampling points of two types.

Results There are seven experiment settings to evaluate the performance and equivariance of our model as shown in the table 1. They are I/I , I/Z , I/R , R/R , $Y/SO(3)$, $SO(3)/SO(3)$. The setting A/B denotes that we train our model on the A part of the dataset and then evaluate it on the B part of the dataset. Following the previous works for $3D$ reconstruction, we use *IoU* and *Chamfer-L1 Distance* as the evaluation metric.

The quantitative results are reported in the table 1, and the qualitative results are shown in figure 7. We compare with two other approaches [79] and [75]. We use the provided code with ground truth poses for [79] while we extended the code in [75] for the case of multiple views.

From the table 1, we see that our model outperforms the [79] and [75] by a large margin on I/Z , I/R , and $Y/SO(3)$ settings. Although theoretically, our model is not equivariant to the arbitrary rotation of the object, $Y/SO(3)$ shows the robustness of our model to the object rotation and the generalization ability to some extent. There is still a performance gap between I/I and I/Z . This is because although $SE(2)$ equivariant networks are theoretically strict equivariant, the error in practice is introduced by the finite sampling of the image and the pooling layers. Additionally, we use the ResNet that is equivariant to C_8 approximation of $SO(2)$, which causes this gap but increases the whole pipeline performance in the other tasks. There is not a significant difference between I/Z and I/R , which shows that approximating the spherical field convolution by $SE(2)$ equivariant convolution is reasonable in practice.

In R/R and $SO(3)/SO(3)$ settings, our model surpasses the other models in *IoU*, *Chamfer-L1 Distance* in the chair and car categories while our model is slightly inferior to [79] in the airplane category. It should be noted that while we only need the relative poses of the cameras, our inference in [79] and [75] uses the ground truth poses in relation to the object frame, as well as the explicit positional encoding of the query point in the object frame, which is concatenated to the point feature.

Moreover, in I/I and Y/Y settings, our model has better performance in several experiments. We attribute the superiority to the $SE(3)$ equivariant attention model, which not

Method	chair						
	I/I	I/Z	I/R	R/R	Y/Y	Y/SO(3)	SO(3)/SO(3)
Fvor w/ gt pose [79]	0.691/0.099	0.409/0.253	0.398/0.257	0.669/0.113	0.687/0.103	0.518/0.194	0.664/0.114
DISN w/ gt pose [75]	0.725/0.094	0.335/0.396	0.322/0.405	0.500/0.201	0.659/0.120	0.419/0.303	0.549/0.174
Ours	0.731/0.090	0.631/0.130	0.592/0.137	0.689/0.105	0.698/0.102	0.589/0.142	0.674/0.113
Method	airplane						
	I/I	I/Z	I/R	R/R	Y/Y	Y/SO(3)	SO(3)/SO(3)
Fvor w/ gt pose [79]	0.770/0.051	0.534/0.168	0.533/0.174	0.766/0.053	0.760/0.052	0.579/0.147	0.746/0.056
DISN w/ gt pose [75]	0.752/0.058	0.465/0.173	0.462/0.171	0.611/0.104	0.706/0.069	0.530/0.151	0.631/0.103
Ours	0.773/0.050	0.600/0.092	0.579/0.100	0.759/0.051	0.734/0.052	0.597/0.101	0.722/ 0.056
Method	car						
	I/I	I/Z	I/R	R/R	Y/Y	Y/SO(3)	SO(3)/SO(3)
Fvor w/ gt pose [79]	0.837/0.090	0.466/0.254	0.484/0.258	0.816/0.107	0.830/0.094	0.496/0.240	0.798/0.111
DISN w/ gt pose [75]	0.822/0.089	0.610/0.232	0.567/0.236	0.772/0.135	0.802/0.098	0.614/0.205	0.769/0.123
Ours	0.844/0.081	0.739/0.142	0.741/0.150	0.836/0.089	0.830/0.089	0.744/0.137	0.813/0.097

Table 1. The results for the seven experiments of 8-view 3D reconstruction for the ShapeNet dataset. The metrics in the cell are *IoU* \uparrow and *Chamfer-L1 Distance* \downarrow . We implement [79] and [75] ourselves on our equivariant dataset. For the performance of [75], we follow their work to conduct the multi-view reconstruction by pooling over the feature of every view. The value of *Chamfer-L1 Distance* is multiplied by 10.

Method	w/o SE(2)	w/o conv/trans	w/o dir	Full model
I/I	0.767/0.079	0.695/0.105	0.722/0.093	0.731/0.090
I/Z	0.430/0.234	0.533/0.175	0.553/0.158	0.631/0.130
I/R	0.417/0.249	0.442/0.241	0.466/0.203	0.592/0.137
R/R	0.672/0.112	0.658/0.122	0.682/0.109	0.689/0.105
Y/Y	0.731/0.090	0.644/0.124	0.677/0.111	0.697/0.102
Y/SO(3)	0.467/0.217	0.534/0.170	0.569/0.163	0.589/0.142
SO(3)/SO(3)	0.655/0.120	0.616/0.142	0.636/0.130	0.674/0.113

Table 2. Results for the ablation study: w/o *SE(2)* denotes the model that we replace *SE(2)* equivariant network with conventional CNNs. w/o ray conv/transformer denotes the model where we replace the 2nd (equivariant convolution from the ray space to 3D Euclidean space) and 3rd part (equivariant transformer over the ray space) in our model with max-pooling over features attached to rays going through the same point. w/o dir means the model where we replace the *SE(3)* equivariant attention model with conventional attention. The value of *Chamfer-L1 distance* is multiplied by 10.

only takes the scalar feature but also the directions of the rays into consideration.

Ablation Study We conduct the ablation study on the *SE(2)* convolution as well as the equivariant convolution/transformer parts. We explore the effectiveness of introducing the type-1 order feature compared with the conventional equivariant attention model without positional encoding. We replace the *SE(2)* CNNs backbone with the conventional CNNs to test the power of *SE(2)* CNNs. We replace the equivariant convolution/transformer part with trivial aggregation (max-pooling) combined with MLP. Last, we run an equivariant transformer without using the direction feature while keeping the number of parameters similar to our model.

The table 2 displays the result for the chair category. It illustrates that in the *I/I* and *Y/Y* trials, *SE(2)* CNN is less expressive than traditional CNN, but it contributes to the equivariance of our model looking at the results of *I/Z*, *I/R*, and *Y/SO(3)*. Equivariant ray convolution and transformer (conv/trans) improve both the reconstruction performance and the equivariance outcome. We also compare the ray transformer with a transformer operating only on scalar features without direction, and again we see a drop in performance in every setting, proving the value of taking ray direction into account.

6. Conclusion

We proposed a novel approach for reconstruction from multiple views using equivariant shape priors. This approach bridges the gap between optimization/NeRF based single scene reconstruction and approaches that generalize to new scenes but are not equivariant. We introduced a new mathematical framework for light field convolutions and showed how it is equivalent to intra-view spherical convolutions that we then approximate with *SE(2)*-convolutions. Meanwhile, we propose the equivariant transformer model over the ray space for 3D reconstruction.

References

[1] Jimmy Aronsson. Homogeneous vector bundles and g -equivariant convolutional neural networks. *Sampling Theory, Signal Processing, and Data Analysis*, 20(2):1–35, 2022. 3

[2] Benjamin Attal, Jia-Bin Huang, Michael Zollhöfer, Johannes Kopf, and Changil Kim. Learning neural light fields with ray-space embedding. In *Proceedings of the IEEE/CVF Conference on Computer Vision and Pattern Recognition*, pages 19819–19829, 2022. 2

[3] Miguel Angel Bautista, Walter Talbott, Shuangfei Zhai, Nitish Srivastava, and Joshua M Susskind. On the generalization of learning-based 3d reconstruction. In *Proceedings of the IEEE/CVF Winter Conference on Applications of Computer Vision*, pages 2180–2189, 2021. 2

[4] Erik J Bekkers. B-spline cnns on lie groups. *arXiv preprint arXiv:1909.12057*, 2019. 3

[5] Mojtaba Bemana, Karol Myszkowski, Hans-Peter Seidel, and Tobias Ritschel. X-fields: Implicit neural view-, light-and time-image interpolation. *ACM Transactions on Graphics (TOG)*, 39(6):1–15, 2020. 2

[6] James R Bergen and Edward H Adelson. The plenoptic function and the elements of early vision. *Computational models of visual processing*, 1:8, 1991. 1, 2

[7] Johannes Brandstetter, Rob Hesselink, Elise van der Pol, Erik Bekkers, and Max Welling. Geometric and physical quantities improve $e(3)$ equivariant message passing. *arXiv preprint arXiv:2110.02905*, 2021. 3

[8] Gabriele Cesa, Leon Lang, and Maurice Weiler. A program to build $e(n)$ -equivariant steerable cnns. In *International Conference on Learning Representations*, 2021. 3

[9] Angel X Chang, Thomas Funkhouser, Leonidas Guibas, Pat Hanrahan, Qixing Huang, Zimo Li, Silvio Savarese, Manolis Savva, Shuran Song, Hao Su, et al. Shapenet: An information-rich 3d model repository. *arXiv preprint arXiv:1512.03012*, 2015. 9

[10] Evangelos Chatzipantazis, Stefanos Pertikiozoglou, Edgar Dobriban, and Kostas Daniilidis. Se (3) -equivariant attention networks for shape reconstruction in function space. *arXiv preprint arXiv:2204.02394*, 2022. 3

[11] Anpei Chen, Zexiang Xu, Fuqiang Zhao, Xiaoshuai Zhang, Fanbo Xiang, Jingyi Yu, and Hao Su. Mvsnerf: Fast generalizable radiance field reconstruction from multi-view stereo. In *Proceedings of the IEEE/CVF International Conference on Computer Vision*, pages 14124–14133, 2021. 2

[12] Haiwei Chen, Shichen Liu, Weikai Chen, Hao Li, and Randall Hill. Equivariant point network for 3d point cloud analysis. In *Proceedings of the IEEE/CVF Conference on Computer Vision and Pattern Recognition*, pages 14514–14523, 2021. 3

[13] Jiaxin Chen, Shuo Zhang, and Youfang Lin. Attention-based multi-level fusion network for light field depth estimation. In *Proceedings of the AAAI Conference on Artificial Intelligence*, volume 35, pages 1009–1017, 2021. 2

[14] Ricson Cheng, Ziyan Wang, and Katerina Fragkiadaki. Geometry-aware recurrent neural networks for active visual recognition. *Advances in Neural Information Processing Systems*, 31, 2018. 1

[15] Christopher B Choy, Danfei Xu, JunYoung Gwak, Kevin Chen, and Silvio Savarese. 3d-r2n2: A unified approach for single and multi-view 3d object reconstruction. In *European conference on computer vision*, pages 628–644. Springer, 2016. 2

[16] Taco Cohen, Maurice Weiler, Berkay Kicanaoglu, and Max Welling. Gauge equivariant convolutional networks and the icosahedral cnn. In *International conference on Machine learning*, pages 1321–1330. PMLR, 2019. 3, 16

[17] Taco Cohen and Max Welling. Group equivariant convolutional networks. In *International conference on machine learning*, pages 2990–2999. PMLR, 2016. 3

[18] Taco S Cohen, Mario Geiger, Jonas Köhler, and Max Welling. Spherical cnns. *arXiv preprint arXiv:1801.10130*, 2018. 3, 7

[19] Taco S Cohen, Mario Geiger, and Maurice Weiler. A general theory of equivariant cnns on homogeneous spaces. *Advances in neural information processing systems*, 32, 2019. 3, 4, 5, 8, 18

[20] Congyue Deng, Or Litany, Yueqi Duan, Adrien Poulenard, Andrea Tagliasacchi, and Leonidas Guibas. Vector neurons: A general framework for $so(3)$ -equivariant networks. *arXiv preprint arXiv:2104.12229*, 2021. 3

[21] Carlos Esteves, Christine Allen-Blanchette, Ameesh Makadia, and Kostas Daniilidis. Learning $so(3)$ equivariant representations with spherical cnns. In *Proceedings of the European Conference on Computer Vision (ECCV)*, pages 52–68, 2018. 3, 6, 7

[22] Carlos Esteves, Ameesh Makadia, and Kostas Daniilidis. Spin-weighted spherical cnns. *arXiv preprint arXiv:2006.10731*, 2020. 3, 7

[23] Carlos Esteves, Yinshuang Xu, Christine Allen-Blanchette, and Kostas Daniilidis. Equivariant multi-view networks. In *Proceedings of the IEEE/CVF*

International Conference on Computer Vision, pages 1568–1577, 2019. 3

[24] Marc Finzi, Samuel Stanton, Pavel Izmailov, and Andrew Gordon Wilson. Generalizing convolutional neural networks for equivariance to lie groups on arbitrary continuous data. In *International Conference on Machine Learning*, pages 3165–3176. PMLR, 2020. 3

[25] Marc Finzi, Max Welling, and Andrew Gordon Wilson. A practical method for constructing equivariant multilayer perceptrons for arbitrary matrix groups. *arXiv preprint arXiv:2104.09459*, 2021. 3

[26] Fabian B Fuchs, Daniel E Worrall, Volker Fischer, and Max Welling. Se (3)-transformers: 3d roto-translation equivariant attention networks. *arXiv preprint arXiv:2006.10503*, 2020. 3, 9, 19

[27] Yasutaka Furukawa, Carlos Hernández, et al. Multi-view stereo: A tutorial. *Foundations and Trends® in Computer Graphics and Vision*, 9(1-2):1–148, 2015. 1, 2

[28] Yasutaka Furukawa and Jean Ponce. Accurate, dense, and robust multiview stereopsis. *IEEE transactions on pattern analysis and machine intelligence*, 32(8):1362–1376, 2009. 1

[29] Jean Gallier and Jocelyn Quaintance. *Differential geometry and Lie groups: a computational perspective*, volume 12. Springer Nature, 2020. 3

[30] Michael Goesele, Brian Curless, and Steven M Seitz. Multi-view stereo revisited. In *2006 IEEE Computer Society Conference on Computer Vision and Pattern Recognition (CVPR'06)*, volume 2, pages 2402–2409. IEEE, 2006. 1

[31] Jiaming Han, Jian Ding, Nan Xue, and Gui-Song Xia. Redet: A rotation-equivariant detector for aerial object detection. In *Proceedings of the IEEE/CVF Conference on Computer Vision and Pattern Recognition*, pages 2786–2795, 2021. 10

[32] Stefan Heber and Thomas Pock. Convolutional networks for shape from light field. In *Proceedings of the IEEE Conference on Computer Vision and Pattern Recognition*, pages 3746–3754, 2016. 2

[33] Stefan Heber, Wei Yu, and Thomas Pock. Neural epi-volume networks for shape from light field. In *Proceedings of the IEEE International Conference on Computer Vision*, pages 2252–2260, 2017. 2

[34] Zhicong Huang, Xuemei Hu, Zhou Xue, Weizhu Xu, and Tao Yue. Fast light-field disparity estimation with multi-disparity-scale cost aggregation. In *Proceedings of the IEEE/CVF International Conference on Computer Vision*, pages 6320–6329, 2021. 2

[35] Michael J Hutchinson, Charline Le Lan, Sheheryar Zaidi, Emilien Dupont, Yee Whye Teh, and Hyunjik Kim. Lietransformer: Equivariant self-attention for lie groups. In *International Conference on Machine Learning*, pages 4533–4543. PMLR, 2021. 3

[36] Hae-Gon Jeon, Jaesik Park, Gyeongmin Choe, Jinsun Park, Yunsu Bok, Yu-Wing Tai, and In So Kweon. Accurate depth map estimation from a lenslet light field camera. In *Proceedings of the IEEE conference on computer vision and pattern recognition*, pages 1547–1555, 2015. 2

[37] Hanwen Jiang, Zhenyu Jiang, Kristen Grauman, and Yuke Zhu. Few-view object reconstruction with unknown categories and camera poses. *arXiv preprint arXiv:2212.04492*, 2022. 2

[38] Nima Khademi Kalantari, Ting-Chun Wang, and Ravi Ramamoorthi. Learning-based view synthesis for light field cameras. *ACM Transactions on Graphics (TOG)*, 35(6):1–10, 2016. 2

[39] Abhishek Kar, Christian Häne, and Jitendra Malik. Learning a multi-view stereo machine. *Advances in neural information processing systems*, 30, 2017. 2

[40] Risi Kondor and Shubhendu Trivedi. On the generalization of equivariance and convolution in neural networks to the action of compact groups. In *International Conference on Machine Learning*, pages 2747–2755. PMLR, 2018. 3

[41] Marc Levoy and Pat Hanrahan. Light field rendering. In *Proceedings of the 23rd annual conference on Computer graphics and interactive techniques*, pages 31–42, 1996. 1, 2

[42] Xiaoxiao Long, Cheng Lin, Peng Wang, Taku Komura, and Wenping Wang. Sparseneus: Fast generalizable neural surface reconstruction from sparse views. *arXiv preprint arXiv:2206.05737*, 2022. 2

[43] Lachlan E MacDonald, Sameera Ramasinghe, and Simon Lucey. Enabling equivariance for arbitrary lie groups. In *Proceedings of the IEEE/CVF Conference on Computer Vision and Pattern Recognition*, pages 8183–8192, 2022. 3

[44] Lars Mescheder, Michael Oechsle, Michael Niemeyer, Sebastian Nowozin, and Andreas Geiger. Occupancy networks: Learning 3d reconstruction in function space. In *Proceedings of the IEEE/CVF conference on computer vision and pattern recognition*, pages 4460–4470, 2019. 2

[45] Ben Mildenhall, Pratul P Srinivasan, Rodrigo Ortíz-Cayon, Nima Khademi Kalantari, Ravi Ramamoorthi, Ren Ng, and Abhishek Kar. Local light field fusion: Practical view synthesis with prescriptive sampling guidelines. *ACM Transactions on Graphics (TOG)*, 38(4):1–14, 2019. 2

[46] Ben Mildenhall, Pratul P Srinivasan, Matthew Tancik, Jonathan T Barron, Ravi Ramamoorthi, and Ren Ng. Nerf: Representing scenes as neural radiance fields for view synthesis. *Communications of the ACM*, 65(1):99–106, 2021. 1, 2

[47] David Romero, Erik Bekkers, Jakub Tomczak, and Mark Hoogendoorn. Attentive group equivariant convolutional networks. In *International Conference on Machine Learning*, pages 8188–8199. PMLR, 2020. 3

[48] David W Romero and Jean-Baptiste Cordonnier. Group equivariant stand-alone self-attention for vision. *arXiv preprint arXiv:2010.00977*, 2020. 3

[49] Shunsuke Saito, Zeng Huang, Ryota Natsume, Shigeo Morishima, Angjoo Kanazawa, and Hao Li. Pifu: Pixel-aligned implicit function for high-resolution clothed human digitization. In *Proceedings of the IEEE/CVF International Conference on Computer Vision*, pages 2304–2314, 2019. 1, 2

[50] Victor Garcia Satorras, Emiel Hoogeboom, and Max Welling. E (n) equivariant graph neural networks. In *International conference on machine learning*, pages 9323–9332. PMLR, 2021. 3

[51] Hao Sheng, Pan Zhao, Shuo Zhang, Jun Zhang, and Da Yang. Occlusion-aware depth estimation for light field using multi-orientation epis. *Pattern Recognition*, 74:587–599, 2018. 2

[52] Vincent Sitzmann, Semon Rezhikov, Bill Freeman, Josh Tenenbaum, and Fredo Durand. Light field networks: Neural scene representations with single-evaluation rendering. *Advances in Neural Information Processing Systems*, 34:19313–19325, 2021. 2

[53] Pratul P Srinivasan, Tongzhou Wang, Ashwin Sree-lal, Ravi Ramamoorthi, and Ren Ng. Learning to synthesize a 4d rgbd light field from a single image. In *Proceedings of the IEEE International Conference on Computer Vision*, pages 2243–2251, 2017. 2

[54] Mohammed Suhail, Carlos Esteves, Leonid Sigal, and Ameesh Makadia. Generalizable patch-based neural rendering. *arXiv preprint arXiv:2207.10662*, 2022. 1, 2

[55] Mohammed Suhail, Carlos Esteves, Leonid Sigal, and Ameesh Makadia. Light field neural rendering. In *Proceedings of the IEEE/CVF Conference on Computer Vision and Pattern Recognition*, pages 8269–8279, 2022. 2

[56] Michael W Tao, Sunil Hadap, Jitendra Malik, and Ravi Ramamoorthi. Depth from combining defocus and correspondence using light-field cameras. In *Proceedings of the IEEE International Conference on Computer Vision*, pages 673–680, 2013. 2

[57] Michael W Tao, Jong-Chyi Su, Ting-Chun Wang, Jitendra Malik, and Ravi Ramamoorthi. Depth estimation and specular removal for glossy surfaces using point and line consistency with light-field cameras. *IEEE transactions on pattern analysis and machine intelligence*, 38(6):1155–1169, 2015. 2

[58] Nathaniel Thomas, Tess Smidt, Steven Kearnes, Lusann Yang, Li Li, Kai Kohlhoff, and Patrick Riley. Tensor field networks: Rotation-and translation-equivariant neural networks for 3d point clouds. *arXiv preprint arXiv:1802.08219*, 2018. 3, 9, 19

[59] Yu-Ju Tsai, Yu-Lun Liu, Ming Ouhyoung, and Yung-Yu Chuang. Attention-based view selection networks for light-field disparity estimation. In *Proceedings of the AAAI Conference on Artificial Intelligence*, volume 34, pages 12095–12103, 2020. 2

[60] Shubham Tulsiani, Alexei A Efros, and Jitendra Malik. Multi-view consistency as supervisory signal for learning shape and pose prediction. In *Proceedings of the IEEE conference on computer vision and pattern recognition*, pages 2897–2905, 2018. 2

[61] Michał J Tyszkiewicz, Kevis-Kokitsi Maninis, Stefan Popov, and Vittorio Ferrari. Raytran: 3d pose estimation and shape reconstruction of multiple objects from videos with ray-traced transformers. *arXiv preprint arXiv:2203.13296*, 2022. 2

[62] Soledad Villar, David W Hogg, Kate Storey-Fisher, Weichi Yao, and Ben Blum-Smith. Scalars are universal: Equivariant machine learning, structured like classical physics. *Advances in Neural Information Processing Systems*, 34:28848–28863, 2021. 3

[63] Nanyang Wang, Yinda Zhang, Zhuwen Li, Yanwei Fu, Wei Liu, and Yu-Gang Jiang. Pixel2mesh: Generating 3d mesh models from single rgb images. In *Proceedings of the European conference on computer vision (ECCV)*, pages 52–67, 2018. 1

[64] Qianqian Wang, Zhicheng Wang, Kyle Genova, Pratul P Srinivasan, Howard Zhou, Jonathan T Barron, Ricardo Martin-Brualla, Noah Snavely, and Thomas Funkhouser. Ibrnet: Learning multi-view image-based rendering. In *Proceedings of the IEEE/CVF Conference on Computer Vision and Pattern Recognition*, pages 4690–4699, 2021. 1, 2

[65] Yingqian Wang, Longguang Wang, Zhengyu Liang, Jungang Yang, Wei An, and Yulan Guo. Occlusion-aware cost constructor for light field depth estimation. In *Proceedings of the IEEE/CVF Conference on Computer Vision and Pattern Recognition*, pages 19809–19818, 2022. 2

[66] Sven Wanner and Bastian Goldluecke. Variational light field analysis for disparity estimation and super-

resolution. *IEEE transactions on pattern analysis and machine intelligence*, 36(3):606–619, 2013. 2

[67] Maurice Weiler and Gabriele Cesa. General $e(2)$ -equivariant steerable cnns. *arXiv preprint arXiv:1911.08251*, 2019. 3

[68] Maurice Weiler, Patrick Forré, Erik Verlinde, and Max Welling. Coordinate independent convolutional networks–isometry and gauge equivariant convolutions on riemannian manifolds. *arXiv preprint arXiv:2106.06020*, 2021. 3, 16

[69] Maurice Weiler, Mario Geiger, Max Welling, Wouter Boomsma, and Taco Cohen. 3d steerable cnns: Learning rotationally equivariant features in volumetric data. *arXiv preprint arXiv:1807.02547*, 2018. 3, 5

[70] W Williem and In Kyu Park. Robust light field depth estimation for noisy scene with occlusion. In *Proceedings of the IEEE Conference on Computer Vision and Pattern Recognition*, pages 4396–4404, 2016. 2

[71] Daniel E Worrall, Stephan J Garbin, Daniyar Turmukhametov, and Gabriel J Brostow. Harmonic networks: Deep translation and rotation equivariance. In *Proceedings of the IEEE Conference on Computer Vision and Pattern Recognition*, pages 5028–5037, 2017. 3

[72] Gaochang Wu, Yebin Liu, Lu Fang, and Tianyou Chai. Revisiting light field rendering with deep anti-aliasing neural network. *IEEE Transactions on Pattern Analysis and Machine Intelligence*, 2021. 2

[73] Haozhe Xie, Hongxun Yao, Xiaoshuai Sun, Shangchen Zhou, and Shengping Zhang. Pix2vox: Context-aware 3d reconstruction from single and multi-view images. In *Proceedings of the IEEE/CVF international conference on computer vision*, pages 2690–2698, 2019. 1, 2

[74] Haozhe Xie, Hongxun Yao, Shengping Zhang, Shangchen Zhou, and Wenxiu Sun. Pix2vox++: Multi-scale context-aware 3d object reconstruction from single and multiple images. *International Journal of Computer Vision*, 128(12):2919–2935, 2020. 1, 2

[75] Qiangeng Xu, Weiyue Wang, Duygu Ceylan, Radomir Mech, and Ulrich Neumann. Disn: Deep implicit surface network for high-quality single-view 3d reconstruction. *Advances in Neural Information Processing Systems*, 32, 2019. 1, 2, 10, 11

[76] Yinshuang Xu, Jiahui Lei, Edgar Dobriban, and Kostas Daniilidis. Unified fourier-based kernel and nonlinearity design for equivariant networks on homogeneous spaces. In *International Conference on Machine Learning*, pages 24596–24614. PMLR, 2022. 3, 7

[77] Youze Xue, Jiansheng Chen, Weitao Wan, Yiqing Huang, Cheng Yu, Tianpeng Li, and Jiayu Bao. Mvscrif: Learning multi-view stereo with conditional random fields. In *Proceedings of the IEEE/CVF International Conference on Computer Vision*, pages 4312–4321, 2019. 1

[78] Mingyue Yang, Yuxin Wen, Weikai Chen, Yongwei Chen, and Kui Jia. Deep optimized priors for 3d shape modeling and reconstruction. In *Proceedings of the IEEE/CVF Conference on Computer Vision and Pattern Recognition*, pages 3269–3278, 2021. 2

[79] Zhenpei Yang, Zhile Ren, Miguel Angel Bautista, Zaiwei Zhang, Qi Shan, and Qixing Huang. Fvor: Robust joint shape and pose optimization for few-view object reconstruction. In *Proceedings of the IEEE/CVF Conference on Computer Vision and Pattern Recognition*, pages 2497–2507, 2022. 1, 2, 10, 11

[80] Alex Yu, Vickie Ye, Matthew Tancik, and Angjoo Kanazawa. pixelnerf: Neural radiance fields from one or few images. In *Proceedings of the IEEE/CVF Conference on Computer Vision and Pattern Recognition*, pages 4578–4587, 2021. 1, 2

[81] Shuo Zhang, Hao Sheng, Chao Li, Jun Zhang, and Zhang Xiong. Robust depth estimation for light field via spinning parallelogram operator. *Computer Vision and Image Understanding*, 145:148–159, 2016. 2

A. Proof of Equivalence of Intra-view Light Field Convolution and Spherical Convolution

The $SE(3)$ equivariant convolution over rays transforms into intra-view convolution when the neighboring lights are in the same view. Moreover, the simplified kernel constraint derived in the paper is that for any $(h, t) \in SO(2) \times \mathbb{R}$ and $x = (\mathbf{d}_x, \mathbf{m}_x) \in \mathcal{R}$:

$$\kappa((h, t)x) = \rho_{out}(h)\kappa(x)\rho_{in}(\mathbf{h}_a^{-1}(h, \mathbf{d}_x)),$$

where $\mathbf{h}_a : SO(3) \times \mathbb{S}^2 \rightarrow SO(2)$ is the twist function: $\mathbf{h}_a(g, \mathbf{d}) = s_a(g\mathbf{d})^{-1}gs_a(\mathbf{d})$ for any $g \in SO(3)$ and $\mathbf{d} \in \mathbb{S}^2$.

With the simplified kernel constraint, we can prove that intra-view light field convolution is equivalent to spherical convolution:

$$\begin{aligned} & f^{l_{out}}(x) \\ &= \int_{d(y, \mathbf{c}_x)=0} \kappa(s(x)^{-1}y)\rho_{in}(\mathbf{h}(s(x)^{-1}s(y)))f^{l_{in}}(y)dy \end{aligned} \quad (7)$$

$$\begin{aligned} &= \int_{d(y, \mathbf{c}_x)=0} \kappa(s(x)^{-1}y)\rho_{in}(\mathbf{h}_a(s_a(\mathbf{d}_x)^{-1}s_a(\mathbf{d}_y)))f^{l_{in}}(y)dy \end{aligned} \quad (8)$$

$$\begin{aligned} &= \int_{\mathbf{d}_y \in \mathbb{S}^2} \kappa(s_a(\mathbf{d}_x)^{-1}\mathbf{d}_y, s(x)^{-1}\mathbf{x}_c \times (s_a(\mathbf{d}_x)^{-1}\mathbf{d}_y)) \\ &\quad \rho_{in}(\mathbf{h}_a(s_a(\mathbf{d}_x)^{-1}s_a(\mathbf{d}_y)))f^{l_{in}}(\mathbf{d}_y, \mathbf{c}_x \times \mathbf{d}_y)d\mathbf{d}_y \quad (9) \\ &= \int_{\mathbf{d}_y \in \mathbb{S}^2} \kappa'(s_a(\mathbf{d}(x))^{-1}\mathbf{d}_y)\rho_{in}(\mathbf{h}_a(s_a(\mathbf{d}_x)^{-1}s_a(\mathbf{d}_y))) \\ &\quad f'^{l_{in}}(\mathbf{d}_y)d\mathbf{d}_y. \end{aligned} \quad (10)$$

In line 7, \mathbf{c}_x is the camera center that x goes through.

The line 7 is equal to the line 8 because we assume that the irreducible representation for the translation \mathbb{R} is the identity as mentioned in the paper.

From line 8 to line 9, We can replace $s(x)^{-1}y$ with

$$(s_a(\mathbf{d}_x)^{-1}\mathbf{d}_y, (s(x)^{-1}\mathbf{x}_c) \times (s_a(\mathbf{d}_x)^{-1}\mathbf{d}_y))$$

due to the facts that $s_a(\mathbf{d}_x)^{-1}\mathbf{d}_y = \mathbf{d}_{s(x)^{-1}y}$ and point $s(x)^{-1}\mathbf{x}_c$ is on the ray $s(x)^{-1}y$. Since y goes through \mathbf{c}_x , we can replace y with $(\mathbf{d}_y, \mathbf{c}_x \times \mathbf{d}_y)$.

From line 9 to 10, we have $f'^{l_{in}}(\mathbf{d}_y) = f^{l_{in}}(\mathbf{d}_y, \mathbf{c}_x \times \mathbf{d}_y)$ because \mathbf{c}_x is fixed for any view. Additionally, from line 9 to 10 we replace

$$\kappa(s_a(\mathbf{d}_x)^{-1}\mathbf{d}_y, (s(x)^{-1}\mathbf{x}_c) \times (s_a(\mathbf{d}_x)^{-1}\mathbf{d}_y))$$

with $\kappa'(s_a(\mathbf{d}_x)^{-1}\mathbf{d}_y)$. It is because according to

$$\kappa((h, t)x) = \rho_{out}(h)\kappa(x)\rho_{in}(\mathbf{h}_a^{-1}(h, \mathbf{d}_x)),$$

we have $\kappa((e, t)x) = \kappa(x)$ for any $t \in \mathbb{R}$, where e is the identity element in $SO(2)$; thus when $t = ((-s(x)^{-1}\mathbf{x}_c))^T[0, 0, 1]^T$, we have

$$\begin{aligned} & \kappa(s_a(x)^{-1}\mathbf{d}_y, s(x)^{-1}\mathbf{x}_c \times (s_a(x)^{-1}\mathbf{d}_y)) \\ &= \kappa(s_a(x)^{-1}\mathbf{d}_y, (s(x)^{-1}\mathbf{x}_c + t[0, 0, 1]^T) \times (s_a(x)^{-1}\mathbf{d}_y)) \end{aligned} \quad (11)$$

$$\begin{aligned} &= \kappa((s_a(x)^{-1}\mathbf{d}_y, [0, 0, 0]^T) \\ &= \kappa'((s_a(x)^{-1}\mathbf{d}_y)). \end{aligned} \quad (12)$$

Line 11 is equal to 12 because $s(x)^{-1}\mathbf{x}_c$ is always on the z axis, and thus $s(x)^{-1}\mathbf{x}_c + t[0, 0, 1]^T = [0, 0, 0]^T$.

B. Spherical Convolution Expressed in Gauge Equivariant Convolution Format

Group convolution is a special case of gauge equivariant convolution [68], where gauge equivariant means the equivariance with respect to the transformation of the section map (transformation of the tangent frame). In the following paragraph we give the elaborated definition of gauge equivariance for the sphere.

Suppose $f : \mathbb{S}^2 \rightarrow V$ is the field function corresponding to the section choice $s_a : \mathbb{S}^2 \rightarrow SO(3)$, we use $\mathcal{L}_{s_a \rightarrow s'_a}$ acting on f to denote the change of section map from s_a to s'_a : $(\mathcal{L}_{s_a \rightarrow s'_a}f)(x) = \rho(s_a(x)^{-1}s'_a(x))^{-1}f(x)$, where ρ is the irreducible representation of $SO(2)$ corresponding to the field type of f . The convolution Φ is gauge equivariant when $\Phi(\mathcal{L}_{s_a \rightarrow s'_a}f) = \mathcal{L}_{s_a \rightarrow s'_a}(\Phi(f))$.

In this section, we show that the spherical convolution can be expressed in terms of the gauge equivariant convolution [16], which provides the convenience for us to verify the approximation of spherical convolution through the $SE(2)$ convolution:

$$f^{l_{out}}(x) = \int_{y \in \mathcal{N}(x)} \kappa'(s(x)^{-1}y)\rho_{in}(h_{y \rightarrow x})^{-1}f^{l_{in}}(y)dy,$$

where $\kappa'(hx) = \rho_{out}(h)\kappa'(x)\rho_{in}^{-1}(h)$ for any $h \in SO(2)$.

Since the focus of this section's discussion is spherical convolution, here we use $s(x)$ to denote $s_a(x)$ for any $x \in \mathbb{S}^2$.

For any $x, y \in \mathbb{S}^2$, $s(x)[1, 0, 0]^T, s(x)[0, 1, 0]^T$ attached to x are tangent vectors on x , we parallel transport $s(x)[1, 0, 0]^T$ and $s(x)[0, 1, 0]^T$ along the geodesic between x and y and get two tangent vectors on y , denoted as $s(x \rightarrow y)_1$ and $s(x \rightarrow y)_2$ as shown in the figure 8, where the parallel transport along a smooth curve is a way to translate a vector “parallelly” based on the affine connection, that is, for a smooth curve $\gamma : [0, 1] \rightarrow \mathbb{S}^2$, the parallel transport $X : \text{Im}(\gamma) \rightarrow \mathcal{T}\mathbb{S}^2$ along the curve γ satisfies that $\nabla_{\dot{\gamma}(t)}X = 0$, where $\text{Im}(\gamma) = \{\gamma(t) | t \in [0, 1]\}$ and ∇ is the affine connection.

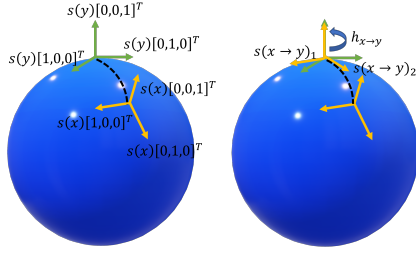


Figure 8. Illustration of $h_{x \rightarrow y}$. $s(x)[1, 0, 0]^T$ and $s(x)[0, 1, 0]^T$ (yellow) attached to x are tangent vectors on x . We parallel transport $s(x)[1, 0, 0]^T$ and $s(x)[0, 1, 0]^T$ along the geodesic (black dashed line) between x and y . The transported tangent vectors need to undergo a transformation $h_{x \rightarrow y}$ in $SO(2)$ to align with the vectors $s(y)[1, 0, 0]^T$ and $s(y)[0, 1, 0]^T$ (green) attached to y .

$s(x \rightarrow y)_1$ and $s(x \rightarrow y)_2$ need to undergo a transformation in $SO(2)$ to align with $s(y)[1, 0, 0]^T$ and $s(y)[0, 1, 0]^T$ on y as shown in the figure 8. We denote the transformation as $h_{x \rightarrow y}$.

With the above notation, the spherical convolution can be expressed as:

$$\begin{aligned} f^{l_{out}}(x) &= \int_{y \in \mathcal{N}(x)} \kappa(s(x)^{-1}y) \rho_{in}(\mathbf{h}(s(x)^{-1}s(y))) f^{l_{in}}(y) dy \\ &= \int_{y \in \mathcal{N}(x)} \kappa(s(x)^{-1}y) \rho_{in}(h_{s(x)^{-1}y \rightarrow \eta}) \\ &\quad \rho_{in}(h_{s(x)^{-1}y \rightarrow \eta})^{-1} \rho_{in}(\mathbf{h}(s(x)^{-1}s(y))) f^{l_{in}}(y) dy \\ &= \int_{y \in \mathcal{N}(x)} \kappa(s(x)^{-1}y) \rho_{in}(h_{s(x)^{-1}y \rightarrow \eta}) \\ &\quad \rho_{in}(h_{y \rightarrow x})^{-1} f^{l_{in}}(y) dy \\ &= \int_{y \in \mathcal{N}(x)} \kappa'(s(x)^{-1}y) \rho_{in}(h_{y \rightarrow x})^{-1} f^{l_{in}}(y) dy, \end{aligned}$$

where $\eta = [0, 0, 1]^T$, the fixed origin point in \mathbb{S}^2 , and $\kappa'(x) = \kappa(x) \rho_{in}(h_{x \rightarrow \eta})^{-1}$ for any $x \in \mathcal{N}(\eta)$.

We can derive the equivariant condition that κ' should satisfy:

$$\begin{aligned} \kappa'(hx) &= \kappa(hx) \rho_{in}(h_{hx \rightarrow \eta})^{-1} \\ &= \rho_{out}(h) \kappa(x) \rho_{in}(\mathbf{h}(h, x))^{-1} \rho_{in}(h_{hx \rightarrow \eta}) \\ &= \rho_{out}(h) \kappa(x) \rho_{in}(h_{x \rightarrow \eta})^{-1} \rho_{in}(h^{-1}) \\ &= \rho_{out}(h) \kappa'(x) \rho_{in}^{-1}(h). \end{aligned}$$

Therefore, the spherical convolution can be expressed as the gauge equivariant convolution format:

$$f^{l_{out}}(x) = \int_{y \in \mathcal{N}(x)} \kappa'(s(x)^{-1}y) \rho_{in}(h_{y \rightarrow x})^{-1} f^{l_{in}}(y) dy,$$

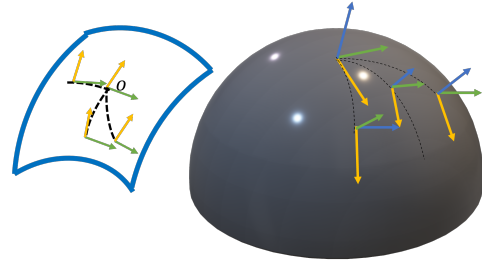


Figure 9. Section choice for every view

where $\kappa'(hx) = \rho_{out}(h) \kappa'(x) \rho_{in}^{-1}(h)$ for any $h \in SO(2)$.

C. Converting Spherical Convolution to $SE(2)$ Equivariant Convolution

As stated in Sec. B, spherical convolution is gauge equivariant with respect to the choice of section map s_a , and the spherical convolution can be written as gauge equivariant convolution. In this section, we use the gauge equivariant convolution to analyze the $SE(2)$ equivariant convolution's approximation of spherical convolution.

Since each view performs spherical convolution on its own, we only analyze the convolution for one view for the sake of simplicity. We use V to denote the space of the rays in the same view, where $V \subset \mathbb{S}^2$. For any $x \in V$, we can choose the section map s_a such that $h_{x \rightarrow o} = e$, where $o \in \mathbb{S}^2$ that o aligns with the optical axis as shown in the figure 9. Again, we use $s(x)$ to denote $s_a(x)$ for any $x \in \mathbb{S}^2$ in this section.

When FOV is small, for any $x, y \in V$, we can have such approximation: $h_{x \rightarrow y} = e$. Then the above gauge equivariant convolution in Sec. B can be approximated as

$$\begin{aligned} f^{l_{out}}(x) &= \int_{y \in \mathcal{N}(x)} \kappa'(s(x)^{-1}y) f^{l_{in}}(y) dy \\ &\xrightarrow{t=s(x)^{-1}y} \int_{t \in \mathcal{N}(\eta)} \kappa'(t) f^{l_{in}}(s(x)t) dt, \end{aligned}$$

where $\eta = [0, 0, 1]^T$, the fixed origin in \mathbb{S}^2 , and $\kappa'(hx) = \rho_{out}(h) \kappa'(x) \rho_{in}^{-1}(h)$ for any $h \in SO(2)$.

Additionally, as illustrated in figure 10, we have a map from V to the projection points on the picture plane represented as $\omega : V \rightarrow \mathbb{R}^2$, where $\omega(o)$ is defined as $[0, 0]^T$. When FOV is small, we have such approximation that for

any $h \in SO(2)$, $t \in \mathcal{N}(\eta)$, and $x \in V$,

$$\omega(s(x)t) \approx \omega(x) + \omega(s(o)t).$$

It is because

$$\omega(s(x)t) = \omega(x) + \omega(s(o)t) + r\left(\frac{\sin\beta_t}{\cos\beta_t} - \frac{\sin\beta_t}{\cos\beta_x \cos(\beta_x + \beta_t)}\right),$$

and we have

$$\begin{aligned} & \lim_{t \rightarrow \eta} r \left(\frac{\sin \beta_t}{\cos \beta_t} - \frac{\sin \beta_t}{\cos \beta_x \cos(\beta_x + \beta_t)} \right) \\ &= r (\tan \beta_x)^2 \beta_t + o(\beta_t^2), \end{aligned}$$

when β_x is small (FOV is small), the approximation stands.

Then $f^{l_{out}}(x) = \kappa'(t)f^{l_{in}}(s(x)t)dt$ can be approximately conducted in the image plane:

$$\begin{aligned}
& f^{l_{out}}(\omega(x)) \\
&= \int_{\omega(s(o)t) \in \mathcal{N}([0,0]^T)} \kappa''(\omega(s(o)t)) f^{l_{in}}(\omega(x) + \omega(s(o)t)) \\
&\quad d(\omega(s(o)t)), \tag{13}
\end{aligned}$$

where for any $x \in \mathbb{S}^2$, $f'(\omega(x)) = f(x)$, and for any $t \in \mathcal{N}(\eta)$, $\kappa''(\omega(s(o)t)) = \kappa'(t)$.

Since for any $h \in SO(2)$ and any $t \in \mathcal{N}(\eta)$, $\omega(s(o)ht) = h\omega(s(o)t)$, we have for any $h \in SO(2)$ and any $t \in \mathcal{N}(\eta)$,

$$\begin{aligned}
\kappa''(h\omega(s(o)t)) &= \kappa''(\omega(s(o)ht)) = \kappa'(ht) \\
&= \rho_{out}(h)\kappa'(t)\rho_{in}^{-1}(h) = \rho_{out}(h)\kappa''(s(o)t)\rho_{in}^{-1}(h) \\
&\stackrel{p=\omega(s(o)t)\in\mathbb{R}^2}{=} k''(hp) \\
&= \rho_{out}(h)\kappa''(p)\rho_{in}^{-1}(h).
\end{aligned}$$

Therefore, convolution 13 is exactly $SE(2)$ equivariant convolution and it can be used to approximate the spherical convolution.

In other words, we can intuitively approximate the equivariant convolution over the partial sphere using the $SE(2)$ equivariant network when the distortion of the sphere and the tangent plane of the optical axis is modest.

D. Proof for Equivariance of Light Field Transformer

The equivariant light field transformer defined in the paper reads:

$$f_2^{out}(x) = \sum_{y \in \mathcal{N}(x)} \frac{\exp(\langle f_q(x, f_2^{in}), f_k(x, y, f_1^{in}) \rangle)}{\sum_{y \in \mathcal{N}(x)} \exp(\langle f_q(x, f_2^{in}) f_k(x, y, f_1^{in}) \rangle)} f_v(x, y, f_1^{in}) \quad (14)$$

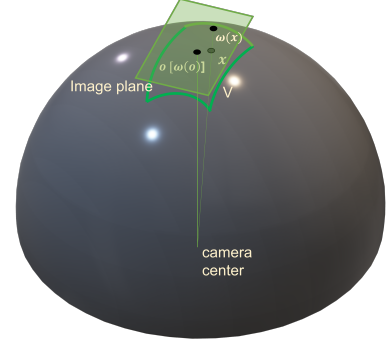


Figure 10. Illustration of projection map ω

is in a general form, where f_2^{out} and f_2^{in} are the output feature and input feature associated with the query point, respectively, and f_1^{in} is the input feature associated with the ray. Again, the subscripts 1 and 2 denote the homogeneous spaces \mathcal{R} and \mathbb{R}^3 , respectively.

According to [19], one can prove that f_q , f_k and f_v are equivariant, that is, for any $g \in SE(3)$, $x \in \mathbb{R}^3$ and $y \in \mathcal{R}$,

$$f_g^{l_{k_j}}(q \cdot x, \mathcal{L}_g^{in}(f_2^{in})) = \rho_2^{l_{k_j}}(\mathbf{h}_2(q^{-1}, q \cdot x)^{-1}) f_g^{l_{k_j}}(x, f_2^{in});$$

$$f_k^{l_{k_j}}(g \cdot x, g \cdot y, \mathcal{L}'^{in}_g(f_1^{in})) = \rho_2^{l_{k_j}}(\mathbf{h}_2(g^{-1}, g \cdot x)^{-1}) f_k^{l_{k_j}}(x, y, f_1^{in});$$

$$f_v^{l_{v_j}}(g \cdot x, g \cdot y, \mathcal{L}'^{in}_q(f_1^{in})) = \rho_2^{l_{v_j}}(\mathbf{h}_2(g^{-1}, g \cdot x)^{-1}) f_v^{l_{v_j}}(x, y, f_1^{in}),$$

where \mathcal{L}^{in} and \mathcal{L}'^{in} are group action of $SE(3)$ on f_2^{in} and f_1^{in} , respectively.

Therefore, $\langle f_q, f_k \rangle = \sum_i (f_q^{l_{k_i}})^T f_k^{l_{k_i}}$ is invariant, which results in the equivariance of the transformer.

E. From $SE(3)$ Equivariant Transformer over Ray Space to $SE(3)$ Equivariant Transformer over Euclidean Space

In our implementation, the attention model is also only applied over the rays going through the points. We can continue to use the interpretation in the convolution from ray space to \mathbb{R}^3 that treats any ray y passing through the point x as a point y' such that $y' - x = d_{s_2(x)^{-1}y}$ as shown in the figure 11.

After we get the initial feature of query points through equivariant convolution from \mathcal{R} to \mathbb{R}^3 , we update the neighboring ray feature by directly concatenating the query point

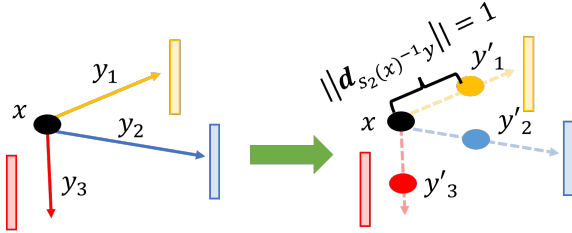


Figure 11. Interpreting rays y_i as points y'_i

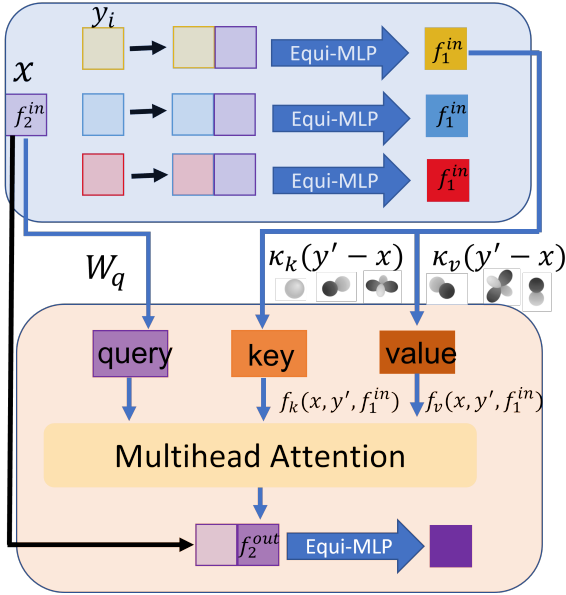


Figure 12. The structures of ray feature update and $SE(3)$ transformer. We treat any ray y going through point x as a point $y' \in \mathbb{R}^3$ such that $y' - x = d_{s_2(x)^{-1}y}$. The blue block indicates the ray feature update, and the pink block is the equivariant attention model. For the ray feature updating, the point feature (lavender) is concatenated to every ray feature (light yellow, light blue and light red), which is the direct sum of features with various types. For the transformer part, we get the query, key, and value feature through the equivariant linear map and apply multi-head attention to obtain the output point feature.

feature to every ray feature before through a $SO(3)$ equivariant MLP as shown in the figure 12. $SO(3)$ equivariant MLP is composed of an equivariant nonlinear layer and self-interaction layer as in the tensor field networks [58].

Since y becomes point y' , and f_1^{in} is the feature over \mathbb{R}^3 attached to ‘‘points’’ y' , it becomes $\oplus_i f_1^{\text{in}_i}$ ⁵. Then transformer 14 would be converted to the transformer in [26] over \mathbb{R}^3 :

⁵Since here f_1^{in} is the fields over \mathbb{R}^3 , we use l instead of l' as the denotation

$$f_2^{\text{out}}(x) = \sum_{y' \in \mathcal{N}(x)} \frac{\exp(\langle f_q(x, f_2^{\text{in}}), f_k(x, y', f_1^{\text{in}}) \rangle)}{\sum_{y' \in \mathcal{N}(x)} \exp(\langle f_q(x, f_2^{\text{in}}) f_k(x, y', f_1^{\text{in}}) \rangle)} f_v(x, y', f_1^{\text{in}}), \quad (15)$$

where the subscript denotes the points to which the feature is attached, i.e., x and y' .

The features f_k, f_v are constructed by the equivariant kernels $\kappa_k = \oplus_{j,i} \kappa_k^{l_{kj}, l_{ini}}, \kappa_v = \oplus_{j,i} \kappa_v^{l_{vj}, l_{ini}}$:

$$f_k^{l_{kj}, l_{ini}}(x, y, f_1^{\text{in}}) = \sum_i \kappa_k^{l_{kj}, l_{ini}}(y' - x) f_1^{l_{ini}}(y);$$

$$f_q^{l_{kj}, l_{ini}}(x, f_2^{\text{in}}) = \sum_i \kappa_v^{l_{vj}, l_{ini}}(y' - x) f_2^{l_{ini}}(y),$$

where for any i, j , any $h_2 \in SO(3)$, and any $x \in \mathbb{R}^3$ $\kappa_k^{l_{kj}, l_{ini}}$ and $\kappa_v^{l_{vj}, l_{ini}}$ should satisfy that:

$$\kappa_k^{l_{kj}, l_{ini}}(h_2 x) = \rho_2^{l_{kj}}(h_2) \kappa_k^{l_{kj}, l_{ini}}(x) \rho_2^{l_{ini}}(h_2^{-1});$$

$$\kappa_v^{l_{vj}, l_{ini}}(h_2 x) = \rho_2^{l_{vj}}(h_2) \kappa_v^{l_{vj}, l_{ini}}(x) \rho_1^{l_{ini}}(h_2^{-1})$$

as stated in [26].

The feature f_q is constructed in the same way as in the transformer 14.

Figure 12 shows the structures of ray feature update and $SE(3)$ equivariant transformer.